Shear response of granular packings compressed above jamming onset

Philip Wang,[1,*] Shiyun Zhang,[1,2,*] Philip Tuckman,[3] Nicholas T. Ouellette ●,[4]
Mark D. Shattuck ●,[5,1] and Corey S. O'Hern ●[1,6,3]

[1]*Department of Mechanical Engineering and Materials Science, Yale University, New Haven, Connecticut 06520, USA*
[2]*Department of Physics, University of Science and Technology of China, Hefei, Anhui 230026, China*
[3]*Department of Physics, Yale University, New Haven, Connecticut 06520, USA*
[4]*Department of Civil and Environmental Engineering, Stanford University, Stanford, California 94305, USA*
[5]*Department of Physics and Benjamin Levich Institute, The City College of the City University of New York, New York, New York 10031, USA*
[6]*Department of Applied Physics, Yale University, New Haven, Connecticut 06520, USA*

We investigate the mechanical response of jammed packings of repulsive, frictionless spherical particles undergoing isotropic compression. Prior simulations of the soft-particle model, where the repulsive interactions scale as a power law in the interparticle overlap with exponent α, have found that the ensemble-averaged shear modulus $\langle G(P) \rangle$ increases with pressure P as $\sim P^{(\alpha-3/2)/(\alpha-1)}$ at large pressures. $\langle G \rangle$ has two key contributions: (1) continuous variations as a function of pressure along geometrical families, for which the interparticle contact network does not change, and (2) discontinuous jumps during compression that arise from changes in the contact network. Using numerical simulations, we show that the form of the shear modulus G^f for jammed packings within near-isostatic geometrical families is largely determined by the affine response $G^f \sim G_a^f$, where $G_a^f/G_{a0} = (P/P_0)^{(\alpha-2)/(\alpha-1)} - P/P_0$, $P_0 \sim N^{-2(\alpha-1)}$ is the characteristic pressure at which $G_a^f = 0$, G_{a0} is a constant that sets the scale of the shear modulus, and N is the number of particles. For near-isostatic geometrical families that persist to large pressures, deviations from this form are caused by significant nonaffine particle motion. We further show that the ensemble-averaged shear modulus $\langle G(P) \rangle$ is not simply a sum of two power laws, but $\langle G(P) \rangle \sim (P/P_c)^a$, where $a \approx (\alpha-2)/(\alpha-1)$ in the $P \to 0$ limit and $\langle G(P) \rangle \sim (P/P_c)^b$, where $b \gtrsim (\alpha-3/2)/(\alpha-1)$, above a characteristic pressure that scales as $P_c \sim N^{-2(\alpha-1)}$.

I. INTRODUCTION

Granular materials, such as collections of grains, bubbles, or other macroscopic particles, interact via highly dissipative forces, which cause these materials to come to rest unless they are continuously driven, e.g., by gravity, shear, or other applied deformations [1]. Further, granular materials transition from fluid- to solidlike states with a nonzero static shear modulus when they are compressed to sufficiently large packing fractions [2]. Despite numerous experimental [3], theoretical [4], and simulation studies [5] of the jamming transition in granular media, there are numerous open questions concerning the structural properties and mechanical response of jammed granular packings.

A simple model for jamming in granular materials is one where we consider frictionless, spherical particles that interact via the pairwise, purely repulsive, finite-ranged ("soft-particle") potential [6,7]

$$U(r_{ij}) = \frac{\epsilon}{\alpha} \left(1 - \frac{r_{ij}}{\sigma_{ij}}\right)^\alpha \Theta\left(1 - \frac{r_{ij}}{\sigma_{ij}}\right), \quad (1)$$

where r_{ij} is the separation between the centers of particles i and j, $\sigma_{ij} = (\sigma_i + \sigma_j)/2$ is the average diameter of particles

i and j, $\Theta(\cdot)$ is the Heaviside step function that prevents particles from interacting if they are not in contact, ϵ is the characteristic energy scale, and α is the power-law scaling exponent of the interaction. For this interaction potential, the onset of jamming in a system with periodic boundary conditions occurs when the number of interparticle contacts N_c first reaches the isostatic value [8], $N_c^0 = dN - d + 1$, where $d = 2, 3$ is the spatial dimension and N is the number of nonrattler particles [9]. As the system is further compressed, the pressure increases from zero.

An important feature of the mechanical response of jammed particle packings is the dependence of the shear modulus G and bulk modulus B on the pressure P under isotropic compression. Prior computational studies of jammed packings of spherical particles have shown that the pressure dependence of the bulk modulus is dominated by the affine response, whereas the pressure dependence of the shear modulus has significant nonaffine contributions [2]. For example, an effective-medium theory, which assumes only affine motion of the particles, predicts that the shear modulus scales as $G(P) \sim P^{1/3}$ for jammed packings of spheres with repulsive Hertzian spring interactions [10] [i.e., $\alpha = 5/2$ in Eq. (1) [11]], whereas experiments and simulations have shown that G increases more strongly than $P^{1/3}$ for packings of Hertzian spheres [7,12,13]. Other studies of sphere packings with repulsive linear spring interactions have shown

that the ensemble-averaged shear modulus is constant at low pressures, $G(P) \sim P^{1/2}$ at high pressures, and the crossover pressure that separates the two scaling regimes decreases as $1/N^2$ with increasing system size [14].

What determines the pressure dependence of the shear modulus as packings of spherical particles are compressed above jamming onset? We have shown in previous studies [15] of jammed packings of spherical particles (with $\alpha = 2$) that the pressure dependence of the shear modulus is controlled by two key contributions: geometrical families [16] and changes in the interparticle contact network [17]. For isotropic compression, jammed packings within a given geometrical family are mechanically stable packings with different pressures that are related to each other via continuous, quasistatic changes in packing fraction with no changes in the contact network. In prior studies [15], we found that the shear modulus G^f within each geometrical family *decreases* with increasing pressure when the interparticle contact network does not change during compression. In these studies, we assumed that (for repulsive linear spring interactions) G^f varies continuously as $G^f(P)/G_0^f = 1 - P/P_0^f$, where $G_0^f = G^f(0)$ and P_0^f is the pressure at which $G^f = 0$. In the present work, we will revisit this assumption and more accurately determine the dependence of G^f on pressure.

Geometrical families begin and end at "point" and "jump changes" in the contact network [17,18]. Point changes involve the addition or removal of a single interparticle contact (or multiple contacts when a rattler is added or removed from the contact network) without significant particle motion. Point changes give rise to a discontinuous jump in the shear modulus for the power-law exponent $\alpha = 2$ in Eq. (1), but not for $\alpha > 2$. In contrast, jump changes correspond to mechanical instabilities [19,20] with multiple simultaneous changes in the contact network and a discontinuous jump in the shear modulus across the jump change for any α. At low pressures, where there are very few changes in the contact network, the geometrical family contribution dominates the ensemble-averaged shear modulus, and thus $\langle G \rangle \sim G_0^f$ for sphere packings with repulsive linear spring interactions in the $P \to 0$ limit. At finite pressure, both geometrical families and changes in the contact network contribute to the pressure dependence of the ensemble-averaged shear modulus.

In this article, we generalize the description of the pressure dependence of the shear modulus for packings of spherical particles compressed above jamming onset to systems with purely repulsive interactions and $\alpha \geqslant 2$, which includes jammed packings of Hertzian spheres. In particular, we characterize the pressure dependence of the shear modulus for geometrical families for near-isostatic packings and decompose the ensemble-averaged shear modulus into contributions from geometrical families and from point and jump changes in the contact network for $\alpha \geqslant 2$.

We find several important results. First, we decompose the shear modulus for each geometrical family G^f into the affine G_a^f and nonaffine G_n^f contributions [20–22], where $G^f = G_a^f - G_n^f$. The affine contribution considers the linear response of the jammed packing to an ideal simple shear deformation without relaxation, whereas the nonaffine contribution includes particle motion from minimization of the total potential energy. We show that the *affine* shear modulus for jammed packings within near-isostatic geometrical families obeys

$$\frac{G_a^f}{G_{a0}(\alpha)} = \left(\frac{P}{P_0(\alpha)}\right)^{\frac{\alpha-2}{\alpha-1}} - \frac{P}{P_0(\alpha)}, \qquad (2)$$

where $G_{a0}(\alpha)$ provides a scale for the shear modulus and $P_0(\alpha)$ is the pressure at which $G_a^f = 0$. The affine shear modulus G_a^f includes two terms: a positive contribution that scales with pressure as $[P/P_0(\alpha)]^{(\alpha-2)/(\alpha-1)}$ and a term that decreases linearly with P.

We next characterize the form for the shear modulus G^f of near-isostatic geometrical families close to point and jump changes in the contact network. We show that when geometrical families persist to large pressures, the nonaffine particle motion becomes large, which causes G^f to deviate from the form in Eq. (2). As shown previously for packings of spherical particles with repulsive linear spring interactions [15], we find that both geometrical families and changes in the contact network determine the scaling of the ensemble-averaged shear modulus at finite pressure for all $\alpha \geqslant 2$. The ensemble-averaged shear modulus scales as $\langle G(P) \rangle \sim P^a$, where $a \sim (\alpha - 2)/(\alpha - 1)$ at low pressures below a characteristic pressure $P_c \sim 1/N^{2(\alpha-1)}$, and $\langle G(P) \rangle \sim P^b$, where $b \gtrsim (\alpha - 3/2)/(\alpha - 1)$ for $P > P_c$. Specifically, for Hertzian spheres, we find that $\langle G(P) \rangle \sim P^{1/3}$ for $P < P_c$ and $\langle G(P) \rangle \sim P^{2/3}$ for $P > P_c$, which is consistent with prior experimental [10] and simulation results [2,7].

The remainder of this article is organized as follows. In Sec. II, we describe the numerical methods used in this study, including the quasistatic, isotropic compression protocol used to generate the jammed packings and the calculations of the pressure, shear stress, and shear modulus for the jammed packings. The key results are presented in Sec. III. We first describe the calculations of the shear modulus as a function of pressure for packings in the first and second geometrical families. We determine analytically the affine contribution to the shear modulus within a given geometrical family and compare the affine shear modulus to the total shear modulus obtained from numerical simulations of sphere packings undergoing quasistatic, isotropic compression. We calculate the ensemble-averaged shear modulus $\langle G \rangle$ as a function of pressure and show how the scaling of $\langle G \rangle$ with pressure varies with the power-law exponent α. For each α, we decompose $\langle G(P) \rangle$ into contributions from geometrical families and changes in the contact network and show that both contributions are important at finite pressure in the large-system limit. In Sec. IV, we summarize our conclusions and suggest future research directions. We also include four Appendixes to provide additional technical details that supplement the main text. In Appendix A, we include a derivation of the decomposition of the shear modulus into the affine and non-affine terms and provide explicit expressions to calculate the nonaffine term [20,22]. In Appendix B, we provide a derivation of the pressure dependence of the affine contribution to the shear modulus of near-isostatic geometrical families. In Appendix C, we calculate the shear modulus for near-isostatic geometrical families as a function of pressure for jammed disk packings with $\alpha = 3$ and for sphere packings with $\alpha = 2$

and 5/2. In Appendix D, we show that since the isostatic geometrical family contribution to the shear modulus includes a strongly negative contribution, the shear modulus can become negative for jammed packings generated at fixed shear strain [23].

II. METHODS

We investigate the mechanical properties of isotropically compressed jammed packings of bidisperse disks in two dimensions (2D) and spheres in 3D, containing $N/2$ large and $N/2$ small particles, each with the same mass m, and diameter ratio $\sigma_l/\sigma_s = 1.4$. The particles are confined within a square or cubic box with side lengths $L_x = L_y = 1$ in 2D or $L_x = L_y = L_z = 1$ in 3D, and periodic boundary conditions in all directions. We consider pairwise, purely repulsive, finite-ranged interactions between particles of the form in Eq. (1), for which the potential energy scales as a power law in the overlap between pairs of particles with exponent α. Pair forces are calculated using $\vec{f}_{ij} = -dU(r_{ij})/dr_{ij}\hat{r}_{ij}$, where $\hat{r}_{ij} = \vec{r}_{ij}/r_{ij}$ is the unit vector vector pointing from the center of particle j to the center of particle i. Results are presented below for $\alpha = 2$ (linear springs), 5/2 (Hertzian springs), and 3. The pressure, shear stress, and shear modulus are expressed in units of ϵ/σ_s^d and forces are expressed in units of ϵ/σ_s below.

We calculate the stress tensor $\hat{\Sigma}$ for each mechanically stable packing using the virial expression [24]

$$\hat{\Sigma}_{\beta\delta} = L^{-d} \sum_{i>j} f_{ij\beta} r_{ij\delta}, \qquad (3)$$

where $\beta, \delta = x, y$, or z, $f_{ij\beta}$ is the β component of the interparticle force $\vec{f}_{ij}$ on particle i due to particle j, and $r_{ij\delta}$ is the δ component of the separation vector $\vec{r}_{ij}$. Note that we exclude rattler particles when calculating $\hat{\Sigma}_{\beta\delta}$. We define the shear stress as $\Sigma = -\hat{\Sigma}_{xy}$ and the pressure as $P = \hat{\Sigma}_{\beta\beta}/d$. To calculate the shear modulus G numerically for each packing, we apply a series of small affine simple shear strain steps, $x_i' = x_i + d\gamma y_i$, to the jammed packing in combination with Lees-Edwards boundary conditions, where $d\gamma = 10^{-9}$ is the shear strain increment, and minimize the total potential energy $U = \sum_{i>j} U(r_{ij})$ using the FIRE algorithm [25] after each applied shear strain. We then measure the static shear modulus $G = d\Sigma/d\gamma$ in the $\gamma \to 0$ limit.

Below, we will characterize the shear modulus as a function of pressure from the onset of jamming near $P = 0$ to systems that are significantly compressed with overlaps $\langle r_{ij} - \sigma_{ij}\rangle/\sigma_{ij} \approx 1\%$. To initialize the system, we randomly place particles in the simulation cell at rest and with no overlaps at packing fraction $\phi < 0.01$. We increase the packing fraction in small increments $d\phi$ by increasing the particle diameters uniformly, and following each compression step, we minimize the total potential energy U. Energy minimization is terminated when $(\sum_i \vec{f}_i/N)^2 < 10^{-32}$, where $\vec{f}_i = \sum_j \vec{f}_{ij}$. Note that energy minimization can terminate when all of the pair forces f_{ij} are near zero (i.e., the system is unjammed) or when the system achieves force balance with nonzero pair forces. After each compression step, we measure the pressure P and compare it to a target pressure P_t. If $P < P_t$, we compress the system by $d\phi$ and minimize the total potential energy. If $P >$

P_t, we return to the system with the lower pressure, reduce the packing fraction increment from $d\phi$ to $d\phi/2$, and compress the system again, and repeat the process. This process is terminated when the pressure satisfies $P_t < P < (1 + \zeta)P_t$, where $\zeta = 10^{-7}$.

We sample more than 1000 jammed packings logarithmically in pressure, spanning from isostatic packings at $P = 10^{-7}$ to compressed states with $P = 10^{-2}$ for $\alpha = 2$. To generate packings of spherical particles interacting via Eq. (1) with $\alpha = 5/2$ and 3, we initialized the system with isostatic packings generated using $\alpha = 2$ and then performed the compression protocol plus energy minimization using the appropriate α. Using the initialization, we have verified that the isostatic contact networks are the same for all α that we studied. For $\alpha = 5/2$ and 3, the pressures that we sample vary from $P = 10^{-10}$ to 10^{-2}.

III. RESULTS

The results concerning the mechanical properties of jammed packings of spherical particles with finite-ranged, purely repulsive interactions are presented in three sections below. In Sec. III A, we investigate the shear modulus $G^{(1)}$ for jammed packings of spherical particles that occur in the *first*, isostatic geometrical families (for power-law exponents $\alpha = 2, 5/2$, and 3 and several system sizes) and determine how $G^{(1)}$ varies with pressure prior to the first change in the interparticle contact network. [Choose $f = 1$ in Eq. (2).] We show that for small pressures, the shear modulus of the first geometrical family, $G^{(1)} \sim G_a^{(1)}$, is given by the affine contribution to the shear modulus. For near-isostatic geometrical families that persist to higher pressures, the nonaffine contribution plays an important role in determining the behavior of $G^{(1)}(P)$ even though the contact network does not change. In Sec. III B, we calculate the pressure-dependent shear modulus of jammed packings that belong to the second geometrical family, i.e., packings that have undergone a change in the contact network and now belong to a different geometrical family than the isostatic one that occurs in the $P \to 0$ limit. In Sec. III C, we determine the ensemble-averaged shear modulus $\langle G \rangle$ and find a master curve for $\langle G(P) \rangle$ as a function of system size. To better understand the pressure dependence, we decompose $\langle G \rangle = \langle G^f \rangle + \langle G^r \rangle$ into contributions from geometrical families G^f and changes in the contact network G^r. We show that in the large-system limit both contributions are important for determining the ensemble-averaged shear modulus $\langle G \rangle$ at finite pressure.

A. Isostatic geometrical families

Isotropically compressed jammed packings occur as geometrical families as a function of pressure. Specifically, if we consider a packing at jamming onset with $P = 0$, it will possess packing fraction ϕ_J, nonrattler particle positions $\vec{R} = \{x_1, x_2, \ldots, x_N, y_1, y_2, \ldots, y_N\}$ in 2D or $\vec{R} = \{x_1, x_2, \ldots, x_N, y_1, y_2, \ldots, y_N, z_1, z_2, \ldots, z_N\}$ in 3D, and a contact network with an isostatic number of contacts, $N_c = N_c^0$. If we compress the jammed system by $d\phi$ (and minimize the total potential energy), the particle positions will change continuously with $d\phi$ to $\vec{R}'$, the pressure will become nonzero,
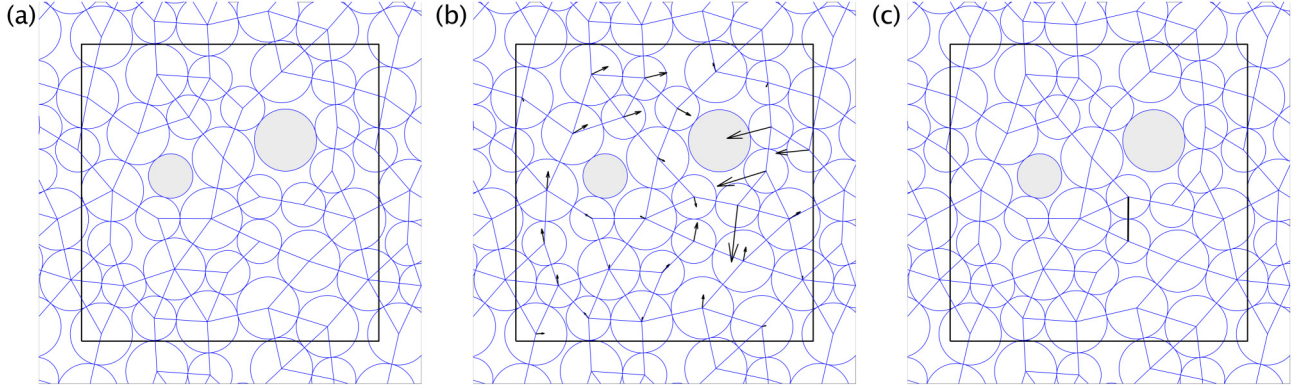
FIG. 1. Snapshots of $N = 32$ jammed disk packings with repulsive linear spring interactions [$\alpha = 2$ in Eq. (1)] undergoing isotropic compression before and after a point change where a new contact is added to the contact network (indicated by thin blue lines). In (a), we show an isostatic packing at $P = 10^{-7}$ with $N_c = N_c^0 = 59$ contacts. (b) The packing in (a) has been compressed to $P = 4.60 \times 10^{-6}$ without any changes in the contact network. The vectors indicate the displacements of the particle centers relative to the packing in (a) after multiplying by 100. (c) The packing in (c) has been compressed to $P = 4.65 \times 10^{-6}$, which results in the addition of one contact, $N_c = N_c^0 + 1$, indicated by the thick black line. The shaded particles indicate rattlers.

and as long as $d\phi$ is sufficiently small, the interparticle contact network will not change. At a given pressure P^*, which is different for each isostatic contact network, the contact network will undergo a point change or a jump change [18]. In Fig. 1, we show the contact network for an isostatic jammed packing (with $N = 32$ and $\alpha = 2$) near the onset of jamming (with $P = 10^{-7}$) and immediately before (with $P = 4.60 \times 10^{-6}$) and after (with $P = 4.65 \times 10^{-6}$) a point change. After the point change, the jammed packing has one extra interparticle contact and $N_c = N_c^0 + 1$. This behavior is similar for isotropically compressed packings with larger system sizes, except P^* decreases with increasing system size.

The shear modulus $G^{(1)}$ of isostatic geometrical families can be decomposed into the affine $G_a^{(1)}$ and nonaffine contributions $G_n^{(1)}$ [20,22]: $G^{(1)} = G_a^{(1)} - G_n^{(1)}$. (See Appendix A.) The affine contribution $G_a^{(1)}$ considers the linear response of the jammed packing to an ideal simple shear deformation without relaxation, whereas the nonaffine contribution $G_n^{(1)}$ includes particle motion from minimization of the total potential energy after the applied simple shear strain. In Fig. 2(a), we show the shear modulus $G^{(1)}$ versus pressure P (on logarithmic scales) for isostatic disk packings within each of 50 different geometrical families generated using $N = 32$ and $\alpha = 2$. We find that for each geometrical family, $G^{(1)}$ tends to a constant in the $P \to 0$ limit, and decreases with increasing pressure. Note that the curves in Fig. 2(a) for $G^{(1)}(P)$ end at different pressures P^* where a point or jump change in the contact network occurs. (We find similar results for jammed sphere packings in 3D with $\alpha = 2$ in Appendix C.)

We first compare $G^{(1)}(P)$ [black points in Fig. 2(a)] to the affine contribution to the shear modulus $G_a^{(1)}(P)$ [blue lines in Fig. 2(a)], where $G_a^{(1)}(P)/G_{a0}(2) = 1 - P/P_0(2)$ is derived and the expressions for $G_{a0}(2)$ and $P_0(2)$ are given in Appendix B. On this scale, we do not see large deviations from $G^{(1)} \sim G_a^{(1)}$. (Similar data for jammed disk packings with $\alpha = 5/2$ are shown in Fig. 3.) The probability distributions for the coefficients $P_0(2)$ and $G_{a0}(2)$ for several system sizes are shown in Figs. 4(a) and 5(a). We find that the average

values $\langle P_0(2) \rangle \sim N^{-2}$ and $\langle G_{a0}(2) \rangle \sim N^{-1}$ tend to zero in the large-system limit as shown in the insets to Figs. 4(a) and 5(a).

To investigate $G^{(1)}(P)$ for jammed packings of repulsive Hertzian disks, we start with an isostatic disk packing generated using repulsive linear spring interactions at the lowest pressure we considered, change the interaction potential from $\alpha = 2$ to $5/2$, and minimize the total potential energy. (See the description of the packing-generation protocol in Sec. II.) We verified that each lowest-pressure, isostatic packing for repulsive linear spring interactions gives rise to an isostatic packing for repulsive Hertzian spring interactions. We then repeat (for repulsive Hertzian spring interactions) the same isotropic compression protocol used to generate isostatic geometrical families for systems with $\alpha = 2$. We show the shear modulus $G^{(1)}(P)$ for the isostatic geometrical families for disks with $\alpha = 5/2$ (on logarithmic scales) in Fig. 3(a). In contrast to the results for repulsive linear spring interactions, $G^{(1)} \to 0$ in the $P \to 0$ limit. As we found for $\alpha = 2$, $G^{(1)}$ also decreases at sufficiently large pressures and we do not find significant deviations from $G^{(1)} \sim G_a^{(1)}$ on logarithmic scales. [Similar results for sphere packings in 3D with $\alpha = 5/2$ are shown in Fig. 15(a) in Appendix C.]

Using Eq. (2), we predict $G_a^{(1)}/G_{a0}(3) = [P/P_0(3)]^{1/2} - P/P_0(3)$ for jammed packings of spherical particles with $\alpha = 3$ in isostatic geometrical families. We show $G^{(1)}(P)$ for packings with $\alpha = 3$ in Fig. 16(a) in Appendix C. Thus, from Eq. 2, $G^{(1)}(P)$ tends to zero in the $P \to 0$ limit for all $\alpha > 2$ and after a characteristic pressure that depends on the power-law exponent α and system size N, $G^{(1)}(P)$ decreases linearly with increasing pressure for all α. The $-P/P_0(\alpha)$ term in $G_a^{(1)}$ can give rise to unstable packings with $G^{(1)} < 0$ at finite pressures [23,26,27], but our results emphasize that all jammed packings possess $G^{(1)} > 0$ at sufficiently low pressures. (See Appendix D for statistics of $G^{(1)} < 0$ as a function of pressure and system size for several α values.)

With a more detailed analysis, we can quantify deviations in $G^{(1)}$ from $G_a^{(1)}$ by multiplying both sides of Eq. (2) by
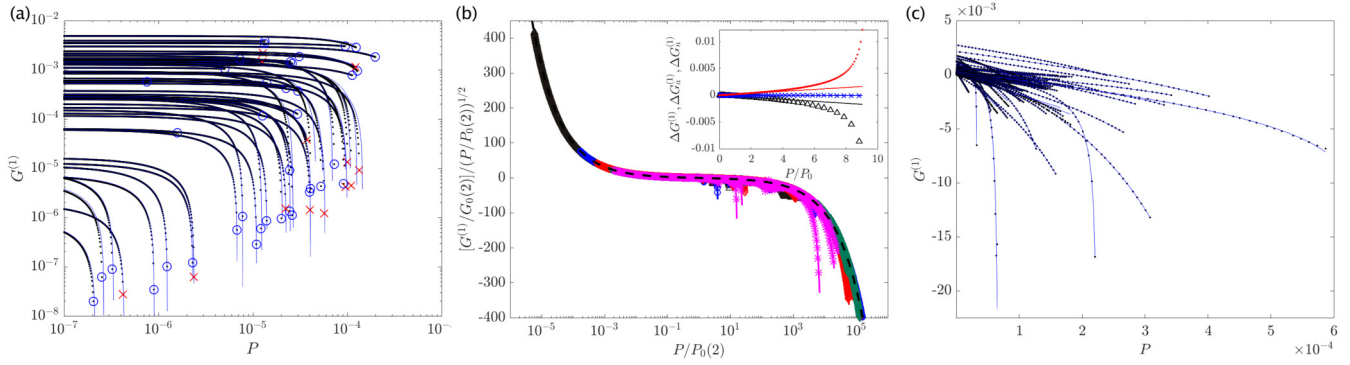
FIG. 2. (a) Shear modulus $G^{(1)}$ vs pressure P (black points) for isostatic packings with $N = 32$ disks within 50 geometrical families that maintain their interparticle contact networks for purely repulsive linear ($\alpha = 2$) spring interactions. The blue lines give the affine contribution $G_a^{(1)}$ [Eq. (2)] for each geometrical family. Blue open circles (red crosses) at the end of $G^{(1)}$ indicate that the packing experienced a point (jump) change at that particular pressure. In this panel, we do not show packings with $G^{(1)} < 0$. (b) $(G^{(1)}/G_0)(P/P_0)^{-1/2}$ for isostatic geometrical families plotted vs P/P_0 for disk packings with repulsive linear ($\alpha = 2$) spring interactions, for several system sizes: $N = 32$ (black upper triangles), 64 (blue circles), 128 (red diamonds), 256 (green downward triangles), and 512 (magenta asterisks). The dashed line is Eq. (4) for $\alpha = 2$ and the solid lines are fits to Eq. (5). In the inset, we show $\Delta G^{(1)} = G^{(1)}(P/P_0) - G^{(1)}(0)$ (black upward triangles), $\Delta G_n^{(1)} = G_n^{(1)}(P/P_0) - G_n^{(1)}(0)$ (red dots), and $\Delta G_a^{(1)} = G_a^{(1)}(P/P_0) - G_a^{(1)}(0)$ (blue ×) with best fits to Eq. (2) (black, red, and blue solid lines, respectively) for an example $N = 32$ packing with $\alpha = 2$. (c) $G^{(1)}$ vs P for the packings in (a) plotted on linear scales (with $G^{(1)} < 0$). The blue lines indicate best fits to Eq. (5) for each geometrical family.

$[P/P_0(\alpha)]^{-(\alpha-3/2)/(\alpha-1)}$ to yield the symmetric form

$$\frac{G^{(1)}}{G_0(\alpha)}\left(\frac{P}{P_0(\alpha)}\right)^{-\frac{\alpha-3/2}{\alpha-1}} = \left(\frac{P}{P_0(\alpha)}\right)^{-\frac{1}{2(\alpha-1)}} - \left(\frac{P}{P_0(\alpha)}\right)^{\frac{1}{2(\alpha-1)}}.$$

(4)

For $P \gg P_0(\alpha)$, the term on the right-hand side of Eq. (4) with the positive exponent will dominate, whereas for $P \ll P_0(\alpha)$, the term with the negative exponent will dominate. In Figs. 2(b) and 3(b), we plot $[G^{(1)}/G_0(\alpha)][P/P_0(\alpha)]^{-(\alpha-3/2)/(\alpha-1)}$ vs $P/P_0(\alpha)$ for packings in isostatic geometrical families with $\alpha = 2$ and 5/2. The

data for $G^{(1)}$ show reasonable collapse onto a master curve (especially at low pressures) for the shear modulus for $\alpha = 2$ and 5/2 for all isostatic packings that we generated.

In Figs. 2(b) and 3(b), we show that $G^{(1)}$ deviates from the dimensionless affine scaling form in Eq. (4) at large P/P_0 for some of the packings with $\alpha = 2$ and 5/2. In the insets to Figs. 2(b) and 3(b), we show that the deviations of $G^{(1)}$ from the scaling form are caused by the growing nonaffine contribution to the shear modulus as the pressure increases. These results are the same for $G^{(1)}$ for all packings that possess deviations at large P/P_0 in Figs. 2(b) and 3(b). Since the nonaffine motion is increasing toward the end of the isostatic
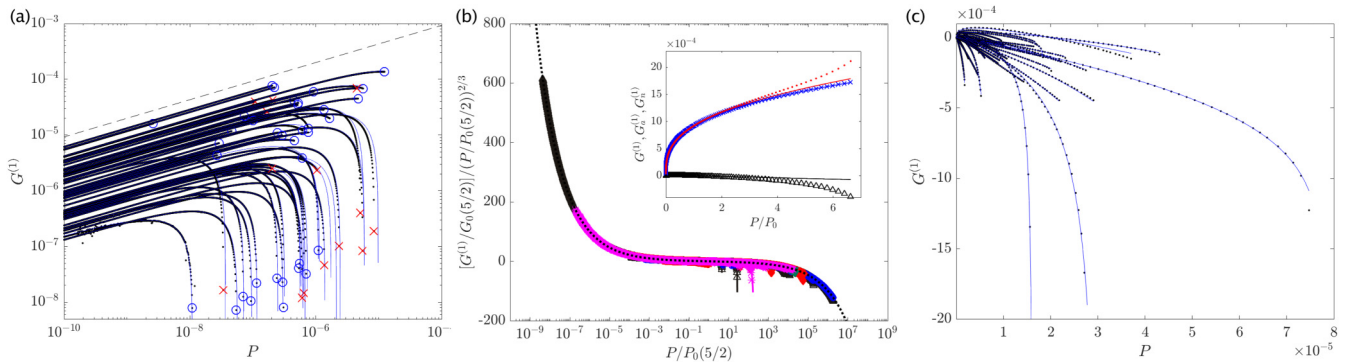
FIG. 3. (a) Shear modulus $G^{(1)}$ vs pressure P (black points) for isostatic packings with $N = 32$ disks within 50 geometrical families that maintain their interparticle contact networks for Hertzian ($\alpha = 5/2$) spring interactions. The blue lines give the affine contribution $G_a^{(1)}$ [Eq. (2)] for each geometrical family. Blue open circles (red crosses) at the end of each $G^{(1)}$ indicate that the packing experienced a point (jump) change at that particular pressure. We do not show packings with $G^{(1)} < 0$. (b) $(G^{(1)}/G_0)(P/P_0)^{-2/3}$ for isostatic geometrical families plotted vs P/P_0 for disk packings with Hertzian ($\alpha = 5/2$) spring interactions, for several system sizes: $N = 32$ (black upper triangles), 64 (blue circles), 128 (red diamonds), 256 (green downward triangles), and 512 (magenta asterisks). The dashed line is Eq. (4) for $\alpha = 5/2$ and the solid lines are fits to Eq. (5) for $\alpha = 5/2$. In the inset, we show $G^{(1)}$ (black upward triangles), $G_n^{(1)}$ (red dots), and $G_a^{(1)}$ (blue ×) with best fits to Eq. (2) (black, red, and blue solid lines, respectively) for an example $N = 32$ packing with $\alpha = 5/2$. (c) $G^{(1)}$ vs P for the packings in (a) plotted on a linear scale (and including packings with $G^{(1)} < 0$). The blue lines indicate best fits to Eq. (5) for each geometrical family.
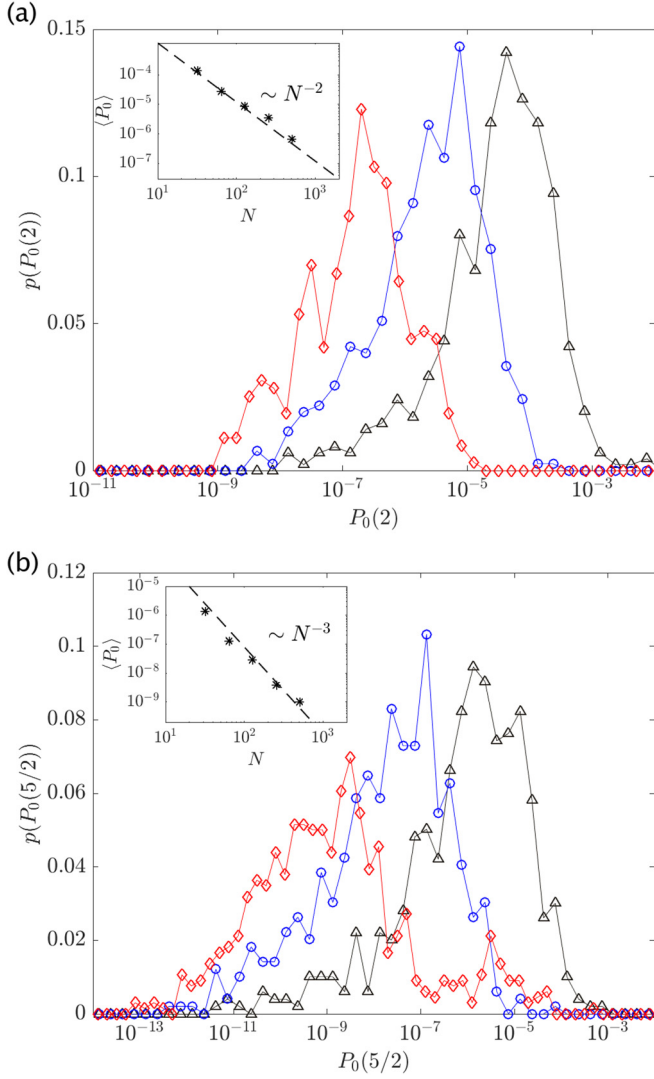
(a)

(b)

FIG. 4. Probability distributions of the characteristic pressure $P_0(\alpha)$ for (a) $\alpha = 2$ and (b) 5/2 for $N = 32$ (black upward triangles), 128 (blue circles), 512 (red diamonds). [$P_0(\alpha)$ was obtained using a best fit of the data for $G^{(1)}$ to Eq. (4).] The insets to (a) and (b) display $\langle P_0 \rangle$ (averaged over geometrical families) vs system size N for $\alpha = 2$ and 5/2, respectively. The dashed lines have slopes equal to -2 and -3 in the insets to (a) and (b).

(a)

(b)

FIG. 5. Probability distributions of the characteristic shear modulus $G_{a0}(\alpha)$ for (a) $\alpha = 2$ and (b) 5/2 for $N = 32$ (black upward triangles), 128 (blue circles), 512 (red diamonds). [$G_{a0}(\alpha)$ was obtained using a best fit of the data for $G^{(1)}$ to Eq. (4).] The insets to (a) and (b) display $\langle G_{a0} \rangle$ (averaged over geometrical families) vs system size N for $\alpha = 2$ and 5/2, respectively. The dashed lines have slopes equal to -1 and -2 in the insets to (a) and (b).

geometrical families, it is likely that it is correlated with a mechanical instability [20,22].

To better capture the shear modulus for isostatic geometrical families $G^{(1)}(P)$ over the full range of pressure, we consider the empirical form

$$\frac{G^{(1)}}{G_0(\alpha)} = \left(\frac{P}{P_0(\alpha)} \right)^{\frac{\alpha-2}{\alpha-1}} - \frac{P}{P_0(\alpha)} \left(\frac{P_0(\alpha) - P_1(\alpha)}{P - P_1(\alpha)} \right)^{\kappa}, \quad (5)$$

where $G^{(1)}[P_0(\alpha)] = 0$ and $P_1(\alpha) > P_0(\alpha)$ is the pressure at which $G^{(1)}$ has an apparent power-law divergence to $-\infty$ with exponent $0 < \kappa < 1$. In Figs. 2(c) and 3(c), we show $G^{(1)}(P)$ for $\alpha = 2$ and 5/2 on a linear scale and include $G^{(1)} < 0$. $G^{(1)}(P)$ decreases roughly linearly with pressure for $P_0 < P \ll P_1$, but then decreases much faster as the pressure approaches P_1 for several of the geometrical families. The
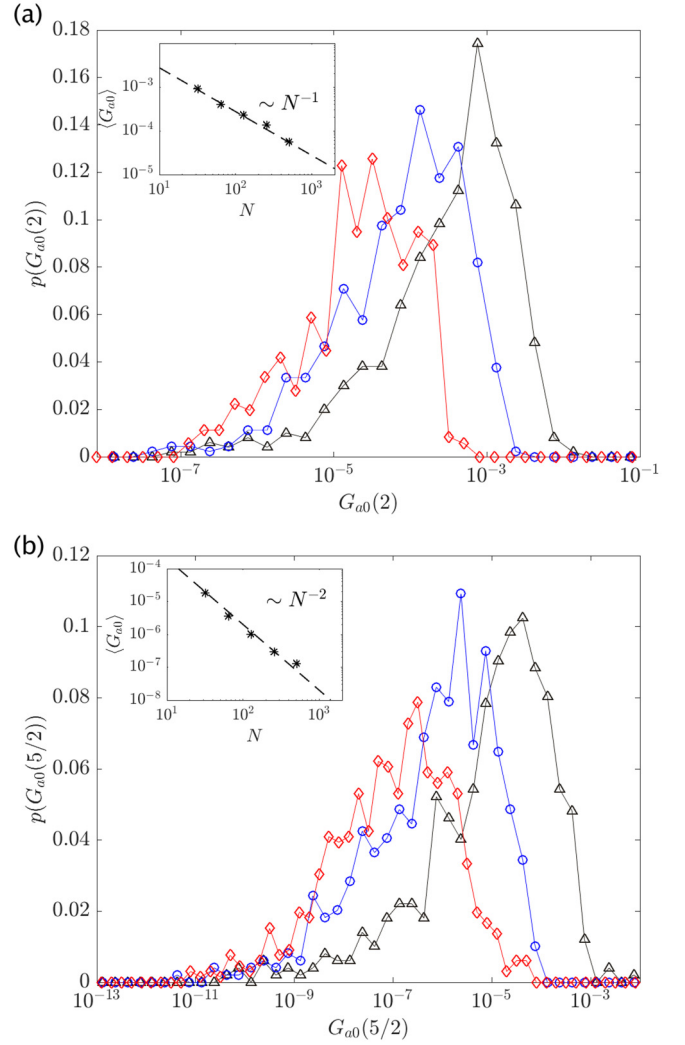
fits of $G^{(1)}(P)$ to Eq. (5) in Figs. 2(c) and 3(c) show that it provides a good description of $G^{(1)}(P)$ over the full range of pressure. The probability distributions for $P_1(\alpha)$ for several system sizes and $\alpha = 2$ and 5/2 are provided in Fig. 6. For some geometrical families, for example, for those where point changes occur at low pressures, $G^{(1)}(P)$ does not deviate significantly from the affine form in Eq. (4) and P_1 is much greater than the pressure range we consider. When we do not include the P_1 values for these geometrical families in the average, we find that $\langle P_1 \rangle \sim \langle P_0 \rangle \sim N^{-2(\alpha-1)}$.

B. Shear modulus for the second geometrical family

In the previous section, we focused on the pressure-dependent shear modulus $G^{(1)}$ of isostatic geometrical families with N_c^0 contacts, prior to the first change in the contact network. In this section, we show preliminary studies of the
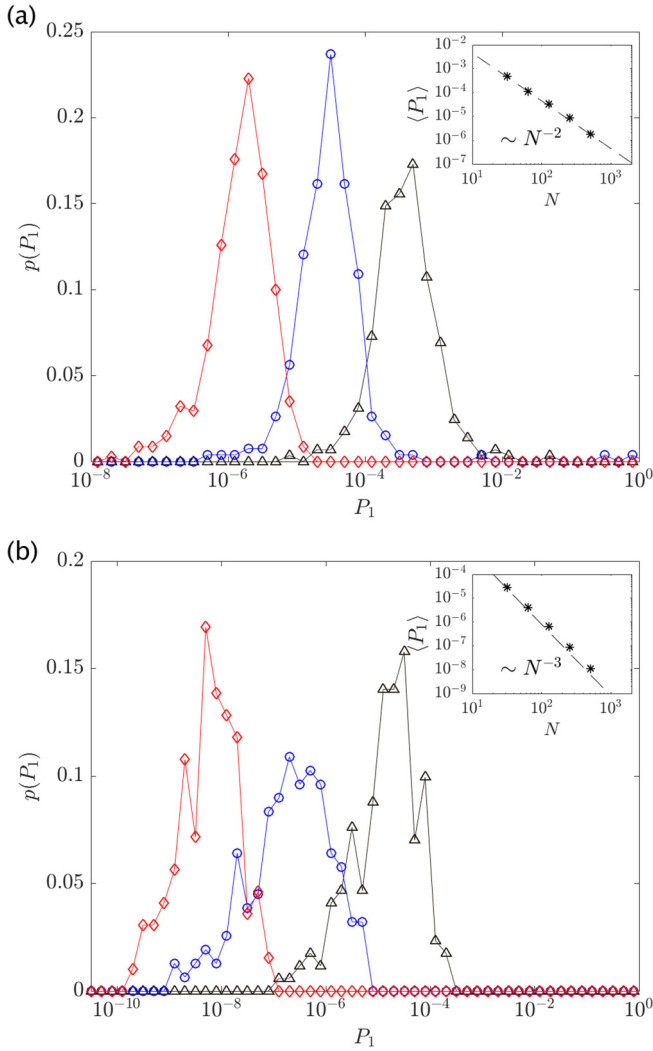
FIG. 6. Probability distributions of the characteristic pressure $P_1(\alpha)$ for (a) $\alpha = 2$ and (b) $5/2$ for $N = 32$ (black upward triangles), 128 (blue circles), 512 (red diamonds). [See Eq. (5) for the definition of $P_1(\alpha)$.] The insets to (a) and (b) display $\langle P_1 \rangle$ (averaged over geometrical families) vs system size N for $\alpha = 2$ and $5/2$, respectively. The dashed lines have slopes equal to -2 and -3 in the insets to (a) and (b).
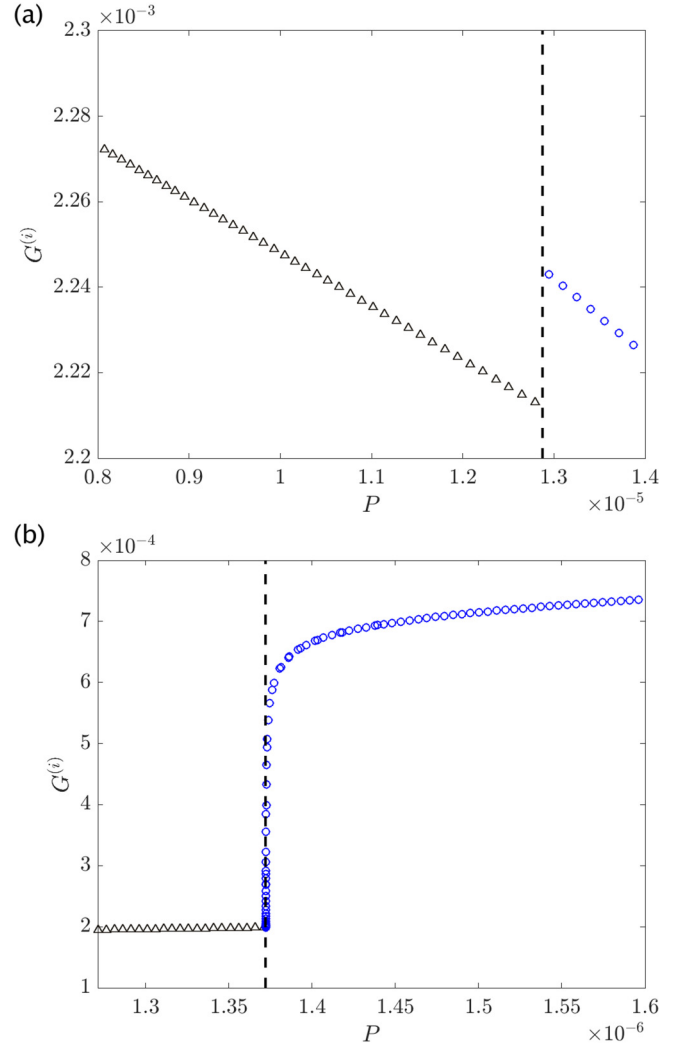

FIG. 7. Shear modulus $G^{(i)}$ of a series of $N = 32$ disk packings with repulsive (a) linear and (b) Hertzian spring interactions as the system undergoes a point change during isotropic compression (at $P \approx 1.29 \times 10^{-5}$ for $\alpha = 2$ and $P = 1.37 \times 10^{-6}$ for $\alpha = 5/2$ indicated by vertical dashed lines) from the isostatic (black upward triangles) geometrical family with N_c^0 contacts to the second geometrical family (blue circles) with $N_c^0 + 1$ contacts.

shear modulus $G^{(2)}$ of the second geometrical family after the packing undergoes a point or jump change in the contact network at P^*. (See Figs. 7 and 8.) We find that when isostatic geometrical families undergo changes in the contact network during isotropic compression, $\approx 75\%$ undergo point changes to a second geometrical family and $\approx 25\%$ undergo jump changes to a second geometrical family for packings with repulsive linear and Hertzian spring interactions. These fractions do not depend strongly on system size. After point changes, nearly all of the packings in the second geometrical families possess $N_c^0 + 1$ contacts. (Note that some point changes correspond to rattler particles that join the contact network, and these point changes cannot be described as an isostatic system that gains a single contact.) For packings (with both $\alpha = 2$ and $5/2$ interactions) that undergo jump changes, $\approx 60\%$ of the packings in the second geometrical

families possess N_c^0 contacts and most of the remaining fraction possess $N_c^0 + 1$ contacts. These results also do not depend strongly on system size.

In Fig. 7, we show the shear modulus $G^{(i)}$ (for the first and second geometrical families) as a function of pressure for a series of disk packings during isotropic compression. At P^*, the disk packing [with $\alpha = 2$ in Fig. 7(a) and $\alpha = 5/2$ in Fig. 7(b)] undergoes a point change and the isostatic geometrical family transitions to a second geometrical family with $N_c^0 + 1$ contacts. As pointed out in our previous studies [18], $G^{(i)}$ is discontinuous across a point change for $\alpha = 2$, but it is continuous across a point change for $\alpha > 2$. For $\alpha = 2$, we find that $G^{(2)}$ for most of the second geometrical families after a point change obey the same scaling form in Eq. (4) for isostatic geometrical families, and the characteristic pressure $P_0 \sim N^{-2}$ and shear modulus $G_0 \sim N^{-1}$ for the second
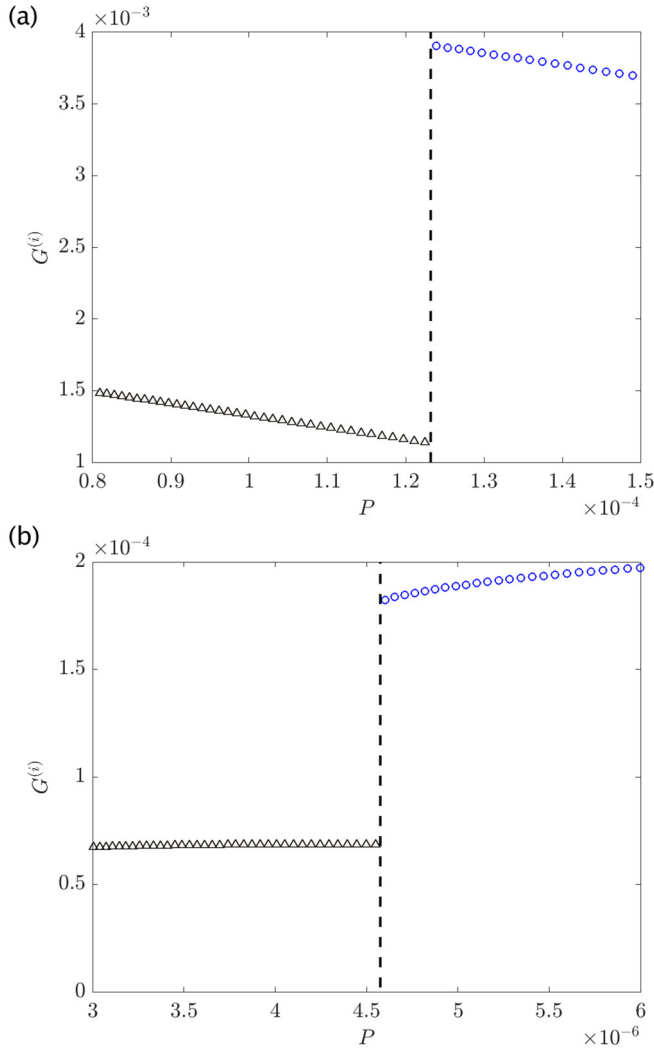
(a)

(b)

FIG. 8. Shear modulus $G^{(i)}$ of a series of $N = 32$ disk packings with repulsive (a) linear and (b) Hertzian spring interactions as the system undergoes a jump change during isotropic compression (at $P \approx 1.23 \times 10^{-4}$ for $\alpha = 2$ and $P = 4.57 \times 10^{-6}$ for $\alpha = 5/2$ indicated by vertical dashed lines) from the isostatic (black upward triangles) geometrical family with N_c^0 contacts to a second geometrical family (blue circles) with $N_c^0 + 1$ contacts.

geometrical families tend to zero in the large-system limit. [See Fig. 9(a).] As we found for the first geometrical families in Fig. 2(b), deviations from Eq. (4) can occur at large pressures $P > P_0$ when $G^{(2)}$ has a significant nonaffine contribution. [See the inset to Fig. 9(a).]

The shear moduli for the second geometrical families, $G^{(2)}$, for packings with $\alpha = 5/2$ after a point change possess deviations from the scaling form in Eq. (4) both at small pressures near the first point change and at large pressures near the second change in the contact network, as shown in Fig. 9(b). For the first geometrical family, there is an important characteristic pressure P_0 that determines when $G^{(1)} = 0$. (For the first geometrical families that persist to large pressures, we also identify a characteristic pressure $P_1 > P^*$, which likely signals an instability of the contact network.) For the second geometrical family following a point change with $\alpha > 2$, there

is another characteristic pressure P^*, indicating the pressure at which the point change from the first to second geometrical family occurs. For highly nonlinear interactions with $\alpha > 2$, the presence of multiple characteristic pressures causes $G^{(2)}$ to deviate from the affine form in Eq. (4). The inset to Fig. 9(b) shows that the deviation of $G^{(2)}$ from the affine scaling form at small pressures is also caused by nonaffine particle motion. The deviations of $G^{(2)}$ from the affine scaling form at large pressures following point changes for $\alpha = 5/2$ are similar to those found for $G^{(1)}$ near the end of the first geometrical family.

As shown in Fig. 8, the shear modulus $G^{(i)}$ is discontinuous when the system undergoes a jump change for packings with all α. If an isostatic geometrical family undergoes a jump change to a second geometrical family, $G^{(2)}$ obeys Eq. (4) for packings with $\alpha = 2$ and $5/2$ over a wide range of pressure. [See Fig. 9(c).] Again, there can be deviations in $G^{(2)}$ from the affine scaling form when the second geometrical family persists to large pressures. In future studies, we will investigate the general form of the shear modulus $G^{(i)}(P)$ for the third-, fourth-, and higher-order geometrical families at elevated pressures.

C. Ensemble-averaged shear modulus

In this section, we investigate the pressure dependence of the ensemble-averaged shear modulus $\langle G \rangle$, which is often studied to mimic the large-system limit. As shown in the previous section, jump changes in the contact network give rise to discontinuities in the shear modulus for packings with all α. In contrast, the shear modulus is continuous across point changes for $\alpha > 2$, but it is discontinuous for $\alpha = 2$. The shear modulus for a single initial condition λ at $P = 0$ undergoing isotropic compression can be written as $G^\lambda = G^{f,\lambda} + G^{r,\lambda}$, where $G^{f,\lambda}$ describes the shear modulus along continuous geometrical families and $G^{r,\lambda}$ includes discontinuities in the shear modulus from point and jump changes. (See Fig. 10.) $G^{r,\lambda}$ for $\alpha = 2$ includes discontinuities in the shear modulus from both point and jump changes, whereas $G^{r,\lambda}$ includes changes in the shear modulus from jump changes only for $\alpha > 2$. The ensemble-averaged shear modulus $\langle G \rangle$ is obtained by averaging over initial conditions λ.

In Fig. 11, we show $\langle G \rangle$, $|\langle G^f \rangle|$, and $\langle G^r \rangle$ for $N = 128$ disk packings with $\alpha = 2$ and $5/2$. At small pressures, $\langle G \rangle \sim \langle G^f \rangle$ since changes in the contact network are rare. In the $P \to 0$ limit, $\langle G \rangle$ is a constant for packings with $\alpha = 2$ and $\langle G \rangle \sim P^{1/3}$ for packings with $\alpha = 5/2$, consistent with the results in Sec. III A. For packings with $\alpha = 2$ and $5/2$, as the pressure increases, $\langle G^f \rangle$ decreases toward zero and at a characteristic pressure, $\langle G \rangle \approx \langle G^r \rangle$. As the pressure continues to increase, $\langle G^f \rangle < 0$ (since the negative contribution to G^f dominates at large pressures), which causes the cusp in $|\langle G^f \rangle|$ in Fig. 11. At large pressures, both $\langle G^f \rangle$ and $\langle G^r \rangle$ contribute to $\langle G \rangle$, and $\langle G \rangle < \langle G^r \rangle$.

In contrast to the affine scaling behavior found for the shear modulus $G^{(1)}$ of isostatic geometrical families, the pressure dependence of the *ensemble-averaged* shear modulus $\langle G \rangle$ is not simply the sum (or difference) of two power laws in pressure [15], $\langle G \rangle \sim AP^a + BP^b$ with exponents a and b. (See Figs. 12 and 13.) To illustrate this, we consider the
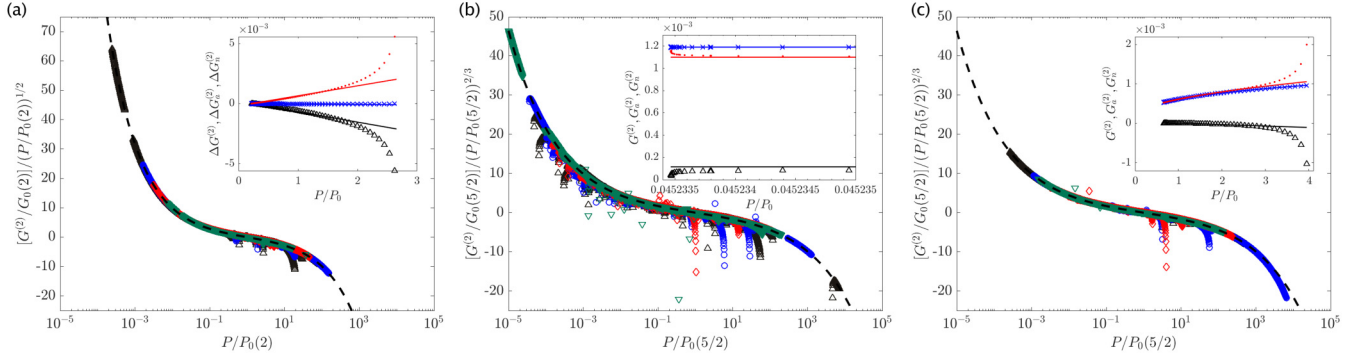
FIG. 9. (a) $(G^{(2)}/G_0)(P/P_0)^{-1/2}$ vs P/P_0 for packings with $\alpha = 2$ in the second geometrical family following a point or jump change in the contact network. $(G^{(2)}/G_0)(P/P_0)^{-2/3}$ is plotted vs P/P_0 for packings with $\alpha = 5/2$ in the second geometrical family following (b) a point change or (c) a jump change in the contact network. In (a)–(c), several system sizes are shown: $N = 32$ (black upper triangles), 64 (blue circles), 128 (red diamonds), 256 (green downward triangles), and 512 (magenta asterisks). The dashed lines in (a)–(c) give Eq. (4) for $\alpha = 2$ in (a) and 5/2 in (b) and (c). In the insets to (a)–(c), we show $\Delta G^{(1)} = G^{(1)}(P/P_0) - G^{(1)}(0)$ or $G^{(1)}(P/P_0)$ (black upward triangles), $\Delta G_n^{(1)} = G_n^{(1)}(P/P_0) - G_n^{(1)}(0)$ or $G_n^{(1)}(P/P_0)$ (red dots), and $\Delta G_a^{(1)} = G_a^{(1)}(P/P_0) - G_a^{(1)}(0)$ or $G_a^{(1)}(P/P_0)$ (blue ×) with best fits to Eq. (2) (black, red, and blue solid lines, respectively) for an example $N = 32$ packing with $\alpha = 2$ [inset to (a)] and 5/2 [insets to (b) and (c)].

dimensionless, symmetric form for $\langle G \rangle$,

$$\frac{\langle G \rangle}{G_c}\left(\frac{P}{P_c}\right)^{-(a+b)/2} = \left(\frac{P}{P_c}\right)^{(a-b)/2} + \left(\frac{P}{P_c}\right)^{-(a-b)/2}, \quad (6)$$

where $G_c = \langle G \rangle(P_c)/2$. Equation (6) is dominated by the $P^{(a-b)/2}$ term for $P < P_c$ and by the $P^{-(a-b)/2}$ term for $P > P_c$. In Figs. 12(a) and 13(a), we plot Eq. (6) as dashed lines for packings with $\alpha = 2$ and 5/2 and compare it to the simulation results for $\frac{\langle G \rangle}{G_c(\alpha)}(\frac{P}{P_c(\alpha)})^{-(a+b)/2}$ for $a \sim (\alpha - 2)/(\alpha - 1)$ and $b \sim (\alpha - 3/2)/(\alpha - 1)$. For packings with both $\alpha = 2$ and 5/2, the simulation data transition between the two limiting power-law behaviors $(P/P_c)^{(a-b)/2}$ and $(P/P_c)^{-(a-b)/2}$ much more abruptly than the sum of the two power laws, $(P/P_c)^{(a-b)/2} + (P/P_c)^{-(a-b)/2}$. To capture this feature in the simulation data, we fit the simulation data for
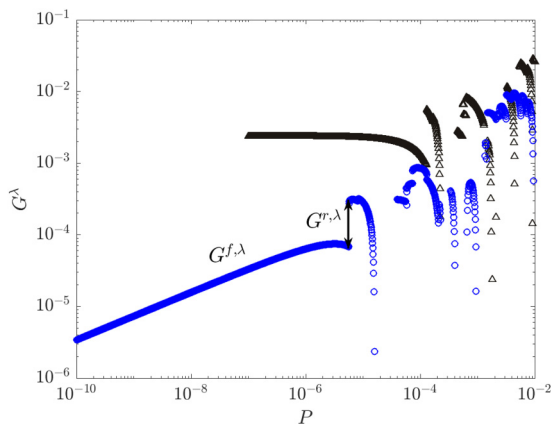

FIG. 10. Shear modulus G^λ for initial condition λ at $P = 0$ undergoing isotropic compression as a function of pressure P for an $N = 32$ packing with repulsive linear (black upward triangles) and Hertzian spring interactions (blue circles). $G^\lambda = G^{f,\lambda} + G^{r,\lambda}$ can be decomposed into the contributions from the continuous geometrical families $G^{f,\lambda}$ and discontinuities $G^{r,\lambda}$ caused by point and jump changes in the contact network.

$\frac{\langle G \rangle}{G_c(\alpha)}(\frac{P}{P_c(\alpha)})^{-(a+b)/2}$ to the p-norm of the right-hand side of Eq. (6), i.e.,

$$\frac{\langle G \rangle}{G_c}\left(\frac{P}{P_c}\right)^{-\frac{a+b}{2}} = \left[\left(\frac{P}{P_c}\right)^{\frac{p(a-b)}{2}} + \left(\frac{P}{P_c}\right)^{-\frac{p(a-b)}{2}}\right]^{\frac{1}{p}}, \quad (7)$$

with $p \sim 2$–5 (~ 2–15) for packings with $N = 32$–512 and $\alpha = 2$ ($\alpha = 5/2$). The p-norm generates polynomials with powers between $(a - b)/2$ and $-(a - b)/2$ to capture the kinklike feature in the simulation data. Fits to Eq. (7) allow us to collapse $\langle G \rangle(P)$ for all of the system sizes studied, as shown in Figs. 12(b) and 13(b). In the insets, we display the exponent $a \sim (\alpha - 2)/(\alpha - 1)$ that controls the low-pressure behavior of $\langle G \rangle$. The exponent $b \gtrsim (\alpha - 3/2)/(\alpha - 1)$ controls the large-pressure behavior. We also find that $P_c \sim N^{-2(\alpha - 1)}$ and $G_c \sim N^{-2(\alpha - 3/2)}$, which is the same system-size dependence as that for P_0 and G_0 for isostatic geometrical families. For $\alpha = 2$, the scaling exponents in the low- and high-pressure limits are $a \sim 0$ and $b \sim 0.60$, and for $\alpha = 5/2$, the scaling exponents in the low- and high-pressure limits are $a \sim 0.36$ and $b \sim 0.70$ [28]. We find similar behavior for $\langle G \rangle$ for jammed sphere packings in 3D for $\alpha = 2$ and 5/2. In the large-α limit, we predict that the scaling exponents in the low- and high-pressure limits will both approach 1.

IV. CONCLUSIONS AND FUTURE DIRECTIONS

The mechanical response of jammed packings of purely repulsive spherical particles to isotropic compression is complex [13,29]. For example, several studies have shown that effective-medium theory, which assumes an affine response to applied deformation, does not accurately predict the behavior of the shear modulus of jammed sphere packings as a function of pressure [7,12]. In addition, simulations of the "soft-particle" model [2], which assumes purely repulsive, finite-ranged interactions between spherical particles that scale as a power law in their overlap with exponent α, have suggested that the ensemble-averaged shear modulus scales
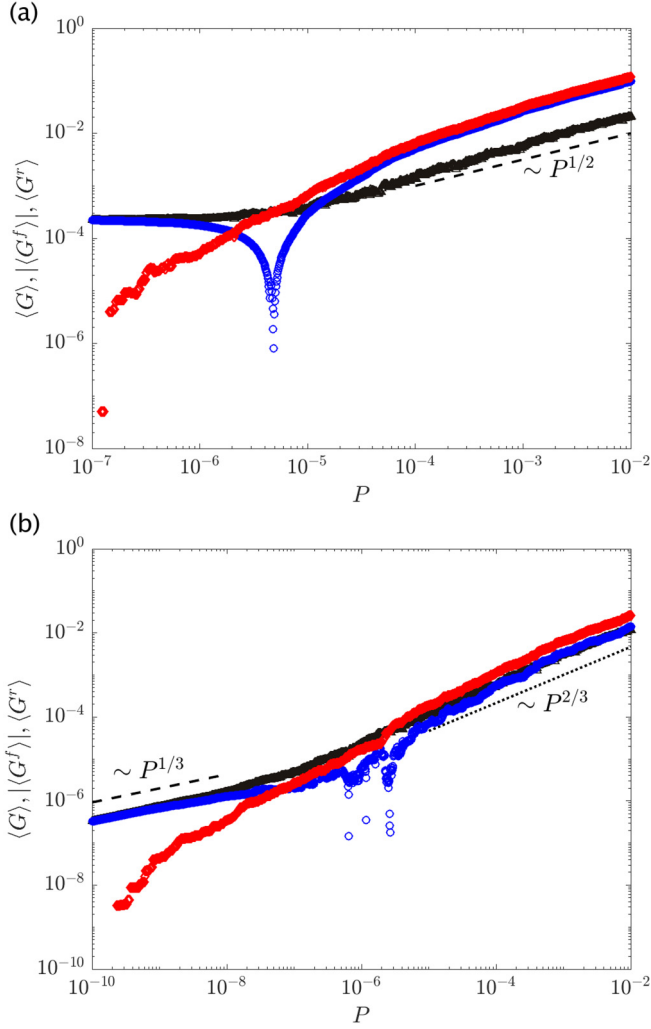
FIG. 11. Ensemble-averaged shear modulus $\langle G \rangle$ (black upward triangles) as a function of pressure P for $N = 128$ packings with (a) $\alpha = 2$ and (b) 5/2 decomposed into contributions from geometrical families $|\langle G^f \rangle|$ (blue circles) and changes in the contact network $\langle G^r \rangle$ (red diamonds). In (a), the dashed line has slope equal to 1/2, and in (b), the dashed and dotted lines have slopes equal to 1/3 and 2/3, respectively.

FIG. 12. (a) Ensemble-averaged shear modulus $(\langle G \rangle / G_c)(P/P_c)^{-(a+b)/2}$ vs P/P_c for jammed disk packings with $\alpha = 2$ and system sizes $N = 32$ (black upward triangles), 64 (blue circles), 128 (red diamonds), 256 (green downward triangles), and 512 (magenta asterisks). The dashed lines have slopes equal to $-1/4$ and $1/4$. The dotted line gives Eq. (6). (b) $\langle G \rangle / G_c$ plotted vs $(P/P_c)^{(a+b)/2}$ for the same data in (a). The solid lines in (a) and (b) are fits to Eq. (7) with $p = 2$–5 for system sizes $N = 32$–512. The upper left inset shows P_c (black asterisks) and G_c (blue circles) vs N. The dotted and dashed lines have slopes equal to -1 and -2, respectively. The lower right inset gives the exponents, a (black upper triangles) and b (blue diamonds), used in fits to Eq. (7) vs N. The horizontal dotted and dashed lines indicate $a = 0$ and $b = 0.5$, respectively.

with pressure as $\langle G \rangle \sim P^{(\alpha - 3/2)/(\alpha - 1)}$. However, the origin of the scaling exponent $(\alpha - 3/2)/(\alpha - 1)$ for the ensemble-averaged shear modulus is not well understood.

In a recent study, we showed that there are two important contributions to the shear modulus in jammed packings of spherical particles undergoing isotropic compression [15]: continuous variations in the shear modulus from geometrical families, for which the interparticle contact network does not change, and discontinuous jumps in the shear modulus from changes in the contact network. In the present work, we show explicitly for $\alpha = 2$, 5/2, and 3 that the form of the shear modulus versus pressure for the first, isostatic geometrical family can be approximated by the affine shear response, i.e., $G^{(1)}/G_0(\alpha) = [P/P_0(\alpha)]^{(\alpha - 2)/(\alpha - 1)} - P/P_0(\alpha)$. However, we observe deviations of $G^{(1)}$ from the affine form when near-isostatic geometrical families persist to large pressures $P > P_0(\alpha)$.
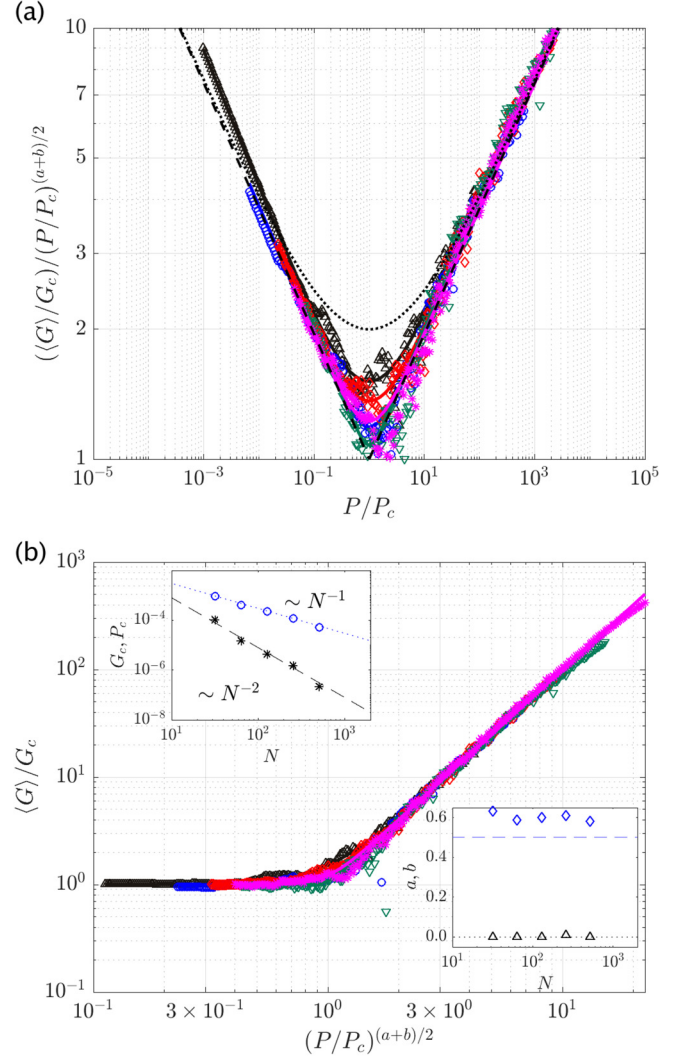
For each initial configuration at $P \sim 0$ that we isotropically compress, we can decompose the shear modulus $G = G^f + G^r$ into contributions from geometrical families (G^f) and from discontinuities arising from point and jump changes in the contact network (G^r). We show that the ensemble-averaged shear modulus $\langle G \rangle \sim \langle G^f \rangle$ at low pressures since changes in the contact network are rare. At larger pressures, the geometrical family contribution is dominated by the $-P$ term (or other negative higher-order terms in P),
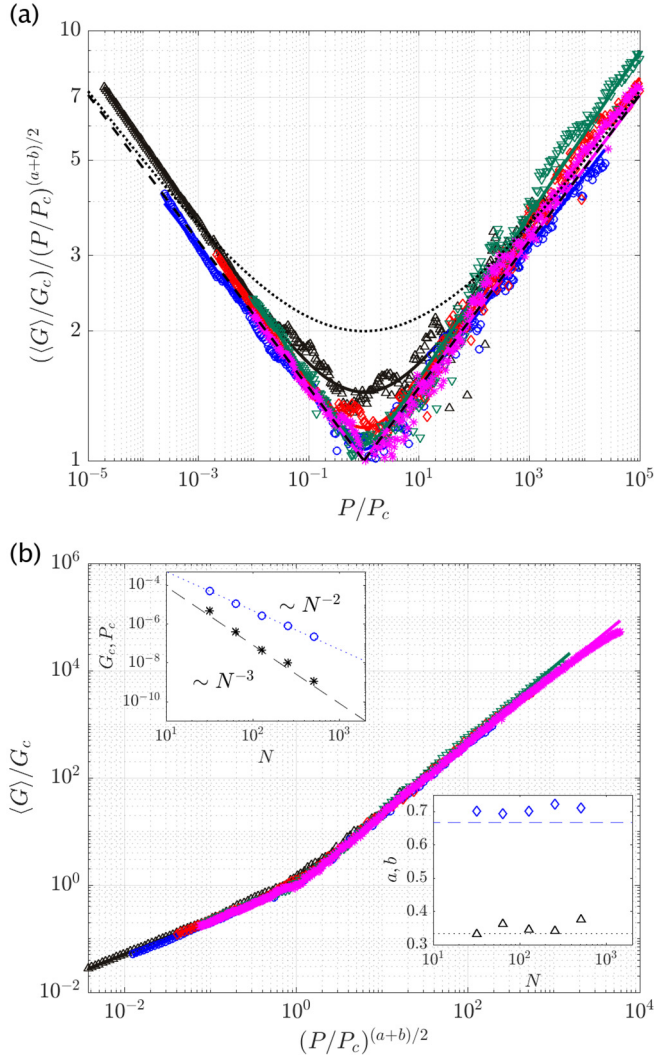
(a)

(b)

FIG. 13. (a) Ensemble-averaged shear modulus $(\langle G \rangle / G_c)(P/P_c)^{-(a+b)/2}$ vs P/P_c for jammed disk packings with $\alpha = 5/2$ and system sizes $N = 32$ (black upward triangles), 64 (blue circles), 128 (red diamonds), 256 (green downward triangles), and 512 (magenta asterisks). The dashed lines have slopes equal to $-1/6$ and $1/6$. The dotted line gives Eq. (6). (b) $\langle G \rangle / G_c$ plotted vs $(P/P_c)^{(a+b)/2}$ for the same data in (a). The solid lines in (a) and (b) are fits to Eq. (7) with $p = 2\text{--}15$ for system sizes $N = 32\text{--}512$. The upper left inset shows P_c (black asterisks) and G_c (blue circles) vs N. The dotted and dashed lines have slopes equal to -2 and -3, respectively. The lower right inset gives the exponents, a (black upper triangles) and b (blue diamonds), used in fits to Eq. (7) vs N. The horizontal dotted and dashed lines indicate $a = 1/3$ and $b = 2/3$, respectively.

$\langle G^f \rangle < 0$, and $\langle G \rangle < \langle G^r \rangle$. We find that both $\langle G^f \rangle$ and $\langle G^r \rangle$ are important for determining $\langle G \rangle$ at finite pressure in the large-system limit. Further, we show that the pressure dependence of $\langle G \rangle$ is not simply a sum of two power laws over the full range of pressure, but $\langle G \rangle \sim P^{(\alpha-2)/(\alpha-1)}$ in the $P \rightarrow 0$ limit, $\langle G \rangle \sim P^b$ at large pressures, where $b \gtrsim (\alpha - 3/2)/(\alpha - 1)$, and the characteristic pressure that separates these scaling regimes, $P_c \sim N^{-1/[2(\alpha-1)]}$, tends to zero in the large-system limit.

This work suggests several areas for future research. First, we investigated the pressure dependence of the shear modulus for the first, isostatic geometrical family and provided preliminary results for the shear modulus of the second geometrical family with $N_c^0 + 1$ contacts. However, we do not yet know the pressure dependence of the shear modulus for higher-order geometrical families that occur at higher pressures. The answer to this question is crucial for developing a theoretical description for the mechanical response of jammed packings undergoing isotropic compression, since the ensemble-averaged shear modulus depends on the pressure dependence of G^f. Second, numerical simulations suggest that the ensemble-averaged shear modulus for packings of frictional spherical particles has a similar pressure dependence as that for packings of frictionless spherical particles, scaling roughly as $\langle G \rangle \sim P^{(\alpha-3/2)/(\alpha-1)}$ at large pressures [30]. However, the separate contributions to the shear modulus from geometrical families and changes in the contact network have not yet been studied for packings of *frictional* spherical particles. Third, several computational studies have shown that $\langle G \rangle \sim P^\eta$ at large pressures for jammed packings of nonspherical particles [31,32] with $\alpha = 2$, where $0.5 < \eta < 1$. These results suggest that the scaling exponent for $\langle G(P) \rangle$ at large pressures depends on both the particle shape [33] (e.g., aspect ratio $\mathcal{A}$) and α. It will be interesting to determine $\eta(\mathcal{A}, \alpha)$ to understand how the rotational degrees of freedom affect the mechanical response of jammed packings of nonspherical particles. Further, for packings of nonspherical particles undergoing isotropic compression, there have not been detailed studies of the separate contributions to $\langle G \rangle$ from geometrical families and from changes in the contact network.

ACKNOWLEDGMENTS

APPENDIX A

In this Appendix, we derive expressions for the affine and nonaffine contributions [20,22] to the shear modulus $G^{(i)}$ of near-isostatic geometrical families. (We consider 2D systems here, but a similar derivation holds for 3D systems.) When we apply an affine simple shear deformation, the particle positions are transformed to $(x_i^a, y_i^a) = (x_i^0 + \gamma y_i^0, y_i^0)$ consistent with Lees-Edwards periodic boundary conditions, where (x_i^0, y_i^0) are the particle positions in the undeformed, reference jammed packing. After each simple shear strain increment γ, we minimize the total potential energy U at constant packing fraction. Thus, after relaxation, the positions of the particles can be written as the sum of an affine term plus a nonaffine

term caused by energy minimization:

$$(x_i', y_i') = (x_i^0 + \gamma y_i^0 + x_i^n, y_i^0 + y_i^n). \qquad (A1)$$

For each reference jammed packing, we can write the total potential energy as a function of the shear strain and nonaffine particle positions, $r_{i\beta}^n$, where $i = 1, 2, \ldots, N$ indicates the particle index and $\beta = x, y$ indicates the Cartesian component of $\vec{r}$. We assume that the jammed disk packing is at a potential energy minimum after each shear strain increment and the total force on each particle remains zero. Thus,

$$f_{i\beta} = -\left(\frac{\partial U}{\partial r_{i\beta}}\right)_\gamma = -\left(\frac{\partial U}{\partial r_{i\beta}^n}\right)_\gamma = 0, \qquad (A2)$$

where $(\cdot)_\gamma$ indicates that the derivatives are evaluated at a fixed shear strain γ. We can then take the derivative of Eq. (A2) with respect to γ,

$$-\frac{df_{i\beta}}{d\gamma} = \left(\frac{\partial^2 U}{\partial r_{i\beta}^n \partial \gamma}\right) + \left(\frac{\partial^2 U}{\partial r_{i\beta}^n \partial r_{j\beta}^n}\right)\frac{dr_{j\beta}^n}{d\gamma}$$

$$= \left(\frac{\partial^2 U}{\partial r_{i\beta}^n \partial \gamma}\right) + \left(\frac{\partial^2 U}{\partial r_{i\beta} \partial r_{j\beta}}\right)\frac{dr_{j\beta}^n}{d\gamma} = 0. \qquad (A3)$$

The shear stress Σ is related to the total derivative of the potential energy with respect to γ:

$$\Sigma L^d = \frac{dU}{d\gamma} = \frac{\partial U}{\partial r_{i\beta}^n}\frac{dr_{i\beta}^n}{d\gamma} + \frac{\partial U}{\partial \gamma} = \frac{\partial U}{\partial \gamma}. \qquad (A4)$$

Note that for a given reference configuration at fixed strain γ, taking derivatives with respect to $r_{i\beta}$ is equivalent to taking derivatives with respect to $r_{i\beta}^n$.

Using Eq. (A3), we can solve for the derivative $dr_{i\beta}^n/d\gamma$,

$$\frac{dr_{i\beta}^n}{d\gamma} = -M_{ij}^{-1}\Xi_{j\beta}, \qquad (A5)$$

where

$$\Xi_{i\beta} = \frac{\partial^2 U}{\partial r_{i\beta}^n \partial \gamma} \qquad (A6)$$

and the Hessian matrix M_{ij} is defined by the second derivatives of the total potential energy U with respect to the particle coordinates,

$$M_{ij} = \frac{\partial^2 U}{\partial r_{i\beta} \partial r_{j\beta}}. \qquad (A7)$$

Using Eq. (A4), we can calculate the shear modulus $GL^d = d\Sigma/d\gamma$,

$$GL^d = \frac{d}{d\gamma}\left(\frac{\partial U}{\partial \gamma} + \frac{\partial U}{\partial r_{i\beta}^n}\frac{dr_{i\beta}^n}{d\gamma}\right) \qquad (A8)$$

$$= \frac{\partial^2 U}{\partial \gamma^2} + \frac{\partial^2 U}{\partial r_{i\beta}^n \partial \gamma}\frac{dr_{i\beta}^n}{d\gamma} \qquad (A9)$$

$$= \frac{\partial^2 U}{\partial \gamma^2} - \Xi_{i\beta}M_{ij}^{-1}\Xi_{j\beta}. \qquad (A10)$$

Thus, we find that the shear modulus $G = G^a - G^n$, where $G^a = L^{-d}\partial^2 U/\partial \gamma^2$ is the affine contribution and

$G^n = L^{-d}\Xi_{i\beta}M_{ij}^{-1}\Xi_{j\beta}$ is the nonaffine contribution. In particular, the shear modulus for each geometrical family can be decomposed as $G^f = G_a^f - G_n^f$.

APPENDIX B

In this Appendix, we calculate the pressure dependence of the affine contribution to the shear modulus G_a^f for geometrical families of near-isostatic jammed packings of spherical particles. We consider packings near jamming onset and apply an affine simple shear shear deformation to their particle coordinates, $(x_i', y_i', z_i') = (x_i^0 + \gamma y_i^0, y_i^0, z_i^0)$ in 3D or $(x_i', y_i') = (x_i^0 + \gamma y_i^0, y_i^0)$ in 2D, where (x_i^0, y_i^0, z_i^0) in 3D and (x_i^0, y_i^0) in 2D are the particle positions in the original jammed packing, consistent with Lees-Edwards boundary conditions for simple shear strain γ. The affine contribution is obtained by calculat-
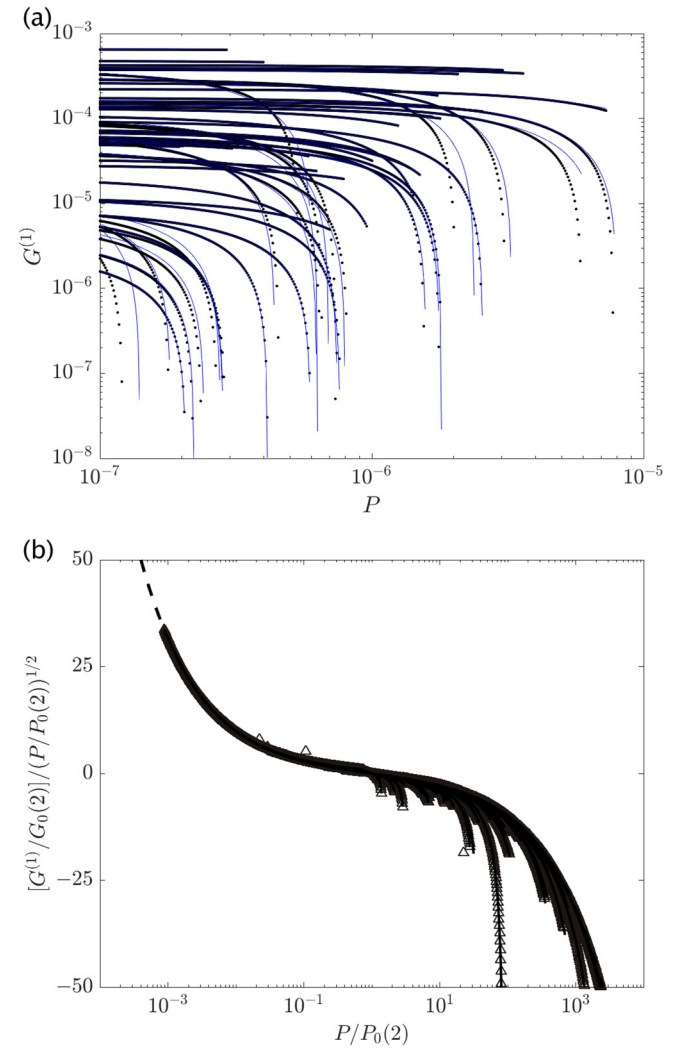

FIG. 14. (a) Shear modulus $G^{(1)}$ within isostatic geometrical families vs pressure P for individual $N = 64$ sphere packings in 3D with $\alpha = 2$ repulsive interactions. The solid blue lines are fits to Eq. (2). (b) $(G^{(1)}/G_0)(P/P_0)^{-1/2}$ plotted vs P/P_0 for the data in (a) and isostatic geometrical families with $G^{(1)} < 0$. The dashed line gives Eq. (4) for $\alpha = 2$, and the solid black lines are fits to Eq. (5).

ing $G_a^f = \partial\Sigma/\partial\gamma$, where the shear stress is given by

$$\Sigma = \epsilon L^{-d} \sum_{i>j} \left(-\frac{x_{ij}y_{ij}}{\sigma_{ij}r_{ij}}\right)\left(1 - \frac{r_{ij}}{\sigma_{ij}}\right)^{\alpha-1}$$

$$\Theta\left(1 - \frac{r_{ij}}{\sigma_{ij}}\right). \tag{B1}$$

In Eq. (B1), x_{ij} and y_{ij} are the x and y separations between the centers of particles i and j. Thus, for the affine contribution, $G_a^f = L^{-d}\partial^2 U/\partial\gamma^2$, we obtain

$$G_a^f = L^{-d}\epsilon \sum_{i>j} \left[-\left(1 - \frac{r_{ij}}{\sigma_{ij}}\right)^{\alpha-1}\frac{y_{ij}^4}{\sigma_{ij}r_{ij}^3}\right.$$

$$\left.+ (\alpha-1)\frac{x_{ij}^2 y_{ij}^2}{\sigma_{ij}^2 r_{ij}^2}\left(1 - \frac{r_{ij}}{\sigma_{ij}}\right)^{\alpha-2}\right]\Theta\left(1 - \frac{r_{ij}}{\sigma_{ij}}\right). \tag{B2}$$

To determine G_a^f as a function of pressure, we write the pressure

$$P = \hat{\Sigma}_{\beta\beta}/d = \frac{\epsilon}{dL^d}\sum_{i>j}\frac{r_{ij}}{\sigma_{ij}}\left(1 - \frac{r_{ij}}{\sigma_{ij}}\right)^{\alpha-1}\Theta\left(1 - \frac{r_{ij}}{\sigma_{ij}}\right)$$

in terms of the particle separations. If we define

$$\overline{P}_{ij} = \epsilon\frac{r_{ij}}{\sigma_{ij}}\left(1 - \frac{r_{ij}}{\sigma_{ij}}\right)^{\alpha-1}\Theta\left(1 - \frac{r_{ij}}{\sigma_{ij}}\right) \tag{B3}$$

and assume that $\overline{P}_{ij}$ scales linearly with pressure for all i, j pairs,

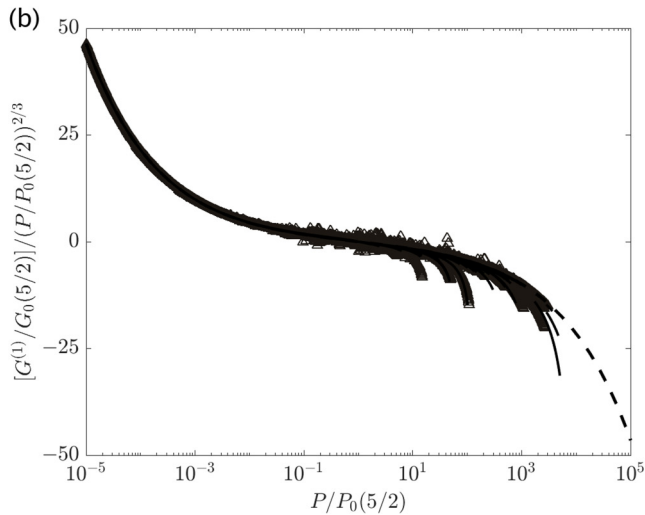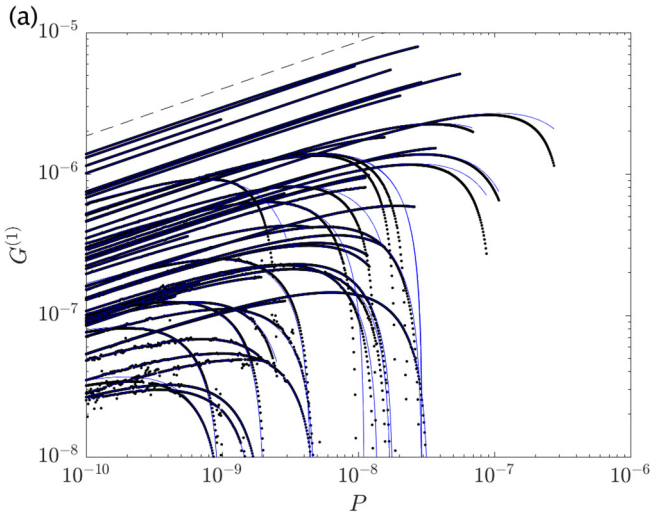$$\overline{P}_{ij} = dL^d\chi_{ij}P, \tag{B4}$$

FIG. 15. Shear modulus $G^{(1)}$ within isostatic geometrical families vs pressure P for individual $N = 64$ sphere packings with $\alpha = 5/2$ repulsive interactions. The solid blue lines are fits to Eq. (2). The dashed line in (a) has a slope equal to 1/3. (b) $(G^{(1)}/G_0)(P/P_0)^{-2/3}$ plotted vs P/P_0 for the data in (a) and isostatic geometrical families with $G^{(1)} < 0$. The dashed line gives Eq. (4) for $\alpha = 5/2$, and the solid black lines are fits to Eq. (5).
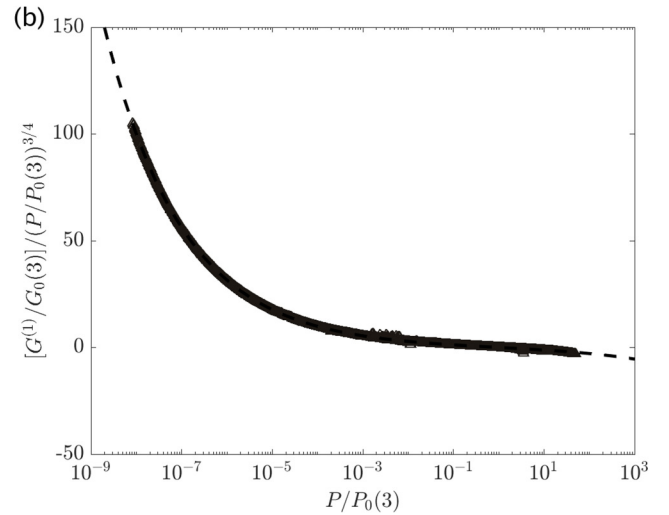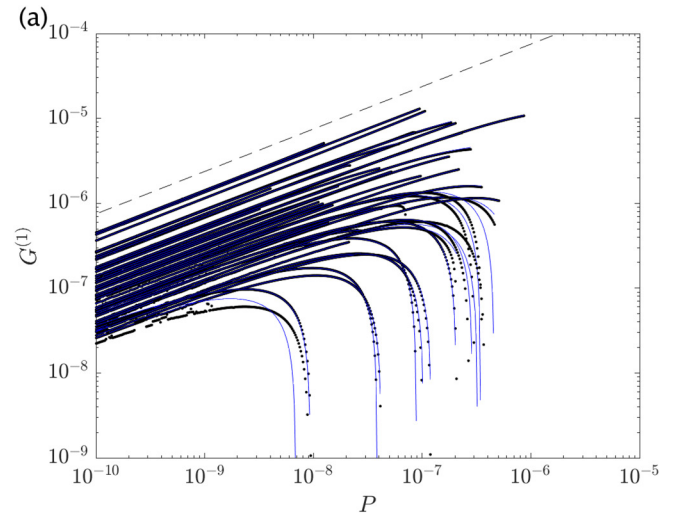

FIG. 16. Shear modulus $G^{(1)}$ within isostatic geometrical families vs pressure P for individual $N = 32$ jammed disk packings with repulsive interactions with power-law exponent $\alpha = 3$ in Eq. (1). The dashed line has a slope equal to 1/2. The solid blue lines are fits to Eq. (2) for each of the 50 geometrical families. (b) $(G^{(1)}/G_0)(P/P_0)^{-3/4}$ plotted vs P/P_0 for the data in (a) and isostatic geometrical families with $G^{(1)} < 0$. The dashed line gives Eq. (4) for $\alpha = 3$, and the solid black lines are fits to Eq. (5).

where χ_{ij} is independent of pressure, we can use Eqs. (B3) and (B4) to express G_a^f in Eq. (B2) as a function of pressure. (We have verified numerically for packings with $\alpha = 2$ and $5/2$ that χ_{ij} is nearly independent of pressure for near-isostatic geometrical families. Deviations only occur near the end of geometrical families.) We find that the affine contribution to the shear modulus for near-isostatic geometrical families is given by

$$G_a^f = L^{-d}(dL^d)^{\frac{\alpha-2}{\alpha-1}} P^{\frac{\alpha-2}{\alpha-1}}$$

$$\times \sum_{i>j}(\alpha-1)\left(\frac{\sigma_{ij}}{r_{ij}}\right)^{\frac{\alpha-2}{\alpha-1}}\frac{x_{ij}^2 y_{ij}^2}{\sigma_{ij}^2 r_{ij}^2}\chi_{ij}^{\frac{\alpha-2}{\alpha-1}}\Theta\left(1-\frac{r_{ij}}{\sigma_{ij}}\right)$$

$$- dP\sum_{i>j}\frac{y_{ij}^4}{r_{ij}^4}\chi_{ij}\Theta\left(1-\frac{r_{ij}}{\sigma_{ij}}\right). \quad (B5)$$

We can express Eq. (B5) in dimensionless form,

$$\frac{G_a^f}{G_{a0}(\alpha)} = \left(\frac{P}{P_0(\alpha)}\right)^{\frac{\alpha-2}{\alpha-1}} - \frac{P}{P_0(\alpha)}, \quad (B6)$$

if we define $G_{a0}(\alpha) = f(\alpha)^{\alpha-1}g^{2-\alpha}$ and $P_0 = [f(\alpha)/g]^{\alpha-1}$, where $f(\alpha) = L^{-d}(dL^d)^{\frac{\alpha-2}{\alpha-1}}\sum_{i>j}(\alpha-1)(\frac{\sigma_{ij}}{r_{ij}})^{\frac{\alpha-2}{\alpha-1}}\frac{x_{ij}^2 y_{ij}^2}{\sigma_{ij}^2 r_{ij}^2}\chi_{ij}^{\frac{\alpha-2}{\alpha-1}}$ $\Theta(1-\frac{r_{ij}}{\sigma_{ij}})$ and $g = d\sum_{i>j}\frac{y_{ij}^4}{r_{ij}^4}\chi_{ij}\Theta(1-\frac{r_{ij}}{\sigma_{ij}})$. Both $f(\alpha)$ and g are roughly independent of pressure and g does not depend on the power-law exponent α. In Eq. (B6), $G_a^f = 0$ when $P = P_0(\alpha)$. For repulsive linear spring interactions, $G_a^f/G_{a0}(2) = 1 - P/P_0(2)$, and for repulsive Hertzian spring interactions, $G_a^f/G_{a0}(5/2) = [P/P_0(5/2)]^{1/3} - P/P_0(5/2)$, as discussed in Sec. III.

APPENDIX C

In this Appendix, we provide the results for the shear modulus for isostatic geometrical families for 2D jammed
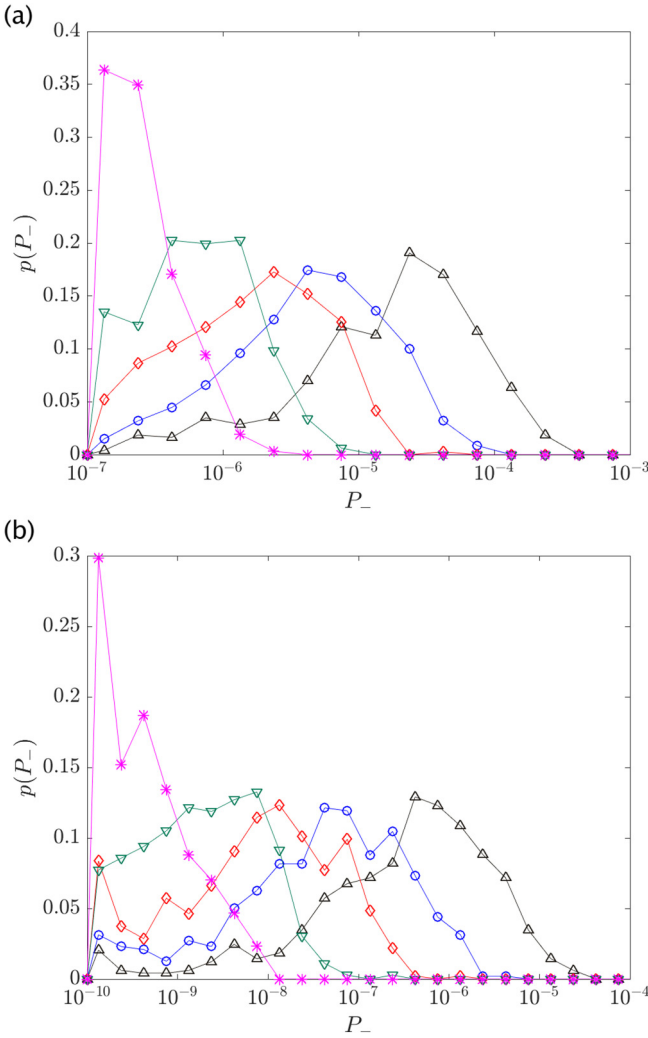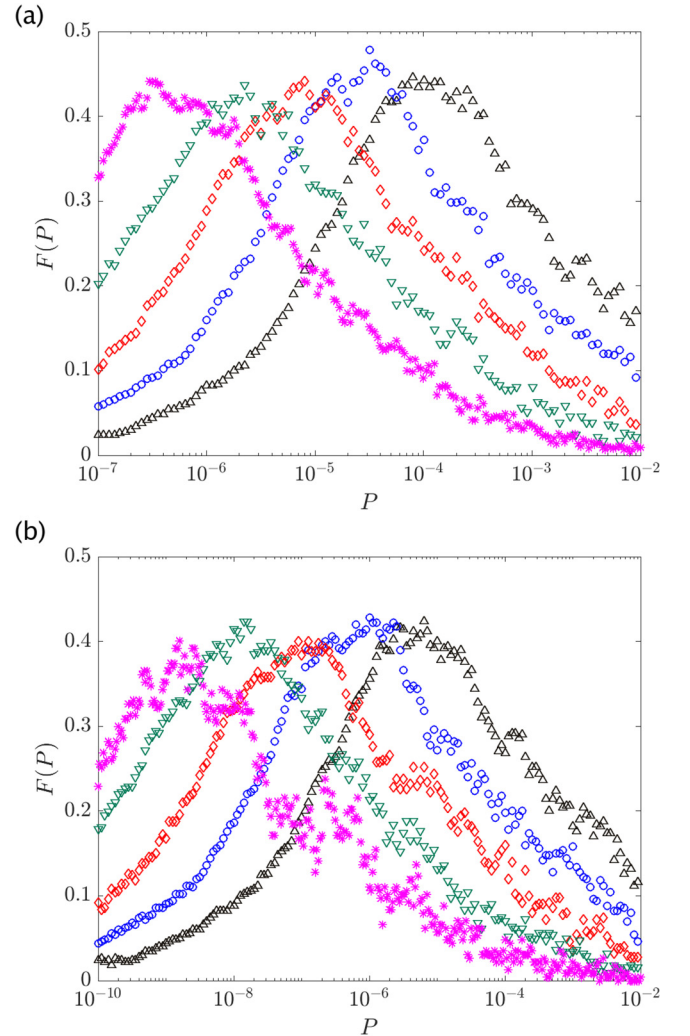

FIG. 17. The probability distribution $p(P_-)$ of the pressure P_- at which the shear modulus for the isostatic geometrical family first becomes negative $G^{(1)} < 0$ for disk packings with (a) $\alpha = 2$ and (b) $5/2$ and system sizes $N = 32$ (black upward triangles), 64 (blue circles), 128 (red diamonds), 256 (green downward triangles), and 512 (magenta asterisks).

FIG. 18. Fraction of packings $F(P)$ at each pressure that possess a negative shear modulus for disk packings with (a) $\alpha = 2$ and (b) $5/2$ and system sizes $N = 32$ (black upward triangles), 64 (blue circles), 128 (red diamonds), 256 (green downward triangles), and 512 (magenta asterisks).

packings of purely repulsive disks with $\alpha = 3$ and 3D jammed packings of purely repulsive spheres with $\alpha = 2$ and $5/2$. In Figs. 14 and 15, we show that $G^{(1)} \sim G_a^{(1)}$ for sphere packings with $\alpha = 2$ and $5/2$. $G^{(1)}$ for $\alpha = 2$ is constant and $G^{(1)}$ for $\alpha = 5/2$ scales as $P^{1/3}$ in the $P \to 0$ limit and $G^{(1)}$ begins decreasing at larger pressures. In Fig. 16, we also show that $G^{(1)}$ for jammed disk packings with $\alpha = 3$ is well approximated by Eq. (2), scaling as $P^{1/2}$ in the $P \to 0$ limit and then decreasing at larger pressures. (Note that for many of the geometrical families for $\alpha = 3$, a change in the contact network occurs before the $-P$ term begins contributing significantly to $G^{(1)}$.)

APPENDIX D

In this Appendix, we quantify the frequency with which disk packings generated using the strain-controlled energy minimization method possess negative shear moduli. (We have verified that all packings generated via isotropic compression, even those with negative shear moduli, possess positive bulk moduli.) The shear modulus for the first geometrical family, $G^{(1)} > 0$ in the $P \to 0$ limit, but it decreases with increasing pressure. Thus, the shear modulus can become negative if a point or jump change in the contact network does not occur abruptly after the start of the first geometrical family. In Fig. 17, we show the distribution $p(P_-)$ of the pressure P_- at which the isostatic geometrical family first becomes negative. We find that $\langle P_- \rangle \sim P_0$ and thus $\langle P_- \rangle$ tends to zero in the large-system limit. $\langle P_- \rangle \sim N^{-2}$ and $\sim N^{-3}$ for packings with $\alpha = 2$ and $5/2$, respectively. After a jump change and after a point change for $\alpha = 2$, the shear modulus for the second geometrical family $G^{(2)}$ jumps discontinuously to either a positive or negative value, depending on the value of $G^{(1)}$ at the end of the first geometrical family and the magnitude and sign of the discontinuous jump in the shear modulus. As the pressure increases, the upward jumps in the shear modulus become larger than the continuous decreases in the shear modulus along geometrical families, and thus the shear modulus remains positive. In Fig. 18, we show the fraction of disk packings $F(P)$ at each pressure with a negative shear modulus. The maximum fraction of packings with negative shear moduli is ≈ 0.4 and occurs at $P_{\max}/P_c \approx 1$. Thus, $P_{\max} \sim N^{-2}$ and $\sim N^{-3}$ for $\alpha = 2$ and $5/2$, respectively.

[1] H. M. Jaeger, S. R. Nagel, and R. P. Behringer, Rev. Mod. Phys. **68**, 1259 (1996).

[2] C. S. O'Hern, L. E. Silbert, A. J. Liu, and S. R. Nagel, Phys. Rev. E **68**, 011306 (2003).

[3] T. S. Majmudar, M. Sperl, S. Luding, and R. P. Behringer, Phys. Rev. Lett. **98**, 058001 (2007).

[4] C. P. Goodrich, A. J. Liu, and J. P. Sethna, Proc. Natl. Acad. Sci. USA **113**, 9745 (2016).

[5] M. P. Ciamarra, R. Pastore, M. Nicodemi, and A. Coniglio, Phys. Rev. E **84**, 041308 (2011).

[6] D. J. Durian, Phys. Rev. Lett. **75**, 4780 (1995).

[7] H. A. Makse, D. L. Johnson, and L. M. Schwartz, Phys. Rev. Lett. **84**, 4160 (2000).

[8] A. V. Tkachenko and T. A. Witten, Phys. Rev. E **60**, 687 (1999).

[9] S. Atkinson, F. H. Stillinger, and S. Torquato, Phys. Rev. E **88**, 062208 (2013).

[10] H. A. Makse, N. Gland, D. L. Johnson, and L. M. Schwartz, Phys. Rev. Lett. **83**, 5070 (1999).

[11] K. L. Johnson and K. L. Johnson, *Contact Mechanics* (Cambridge University Press, Cambridge, UK, 1987).

[12] H. A. Makse, N. Gland, D. L. Johnson, and L. Schwartz, Phys. Rev. E **70**, 061302 (2004).

[13] I. Agnolin and J.-N. Roux, Phys. Rev. E **76**, 061304 (2007).

[14] C. P. Goodrich, A. J. Liu, and S. R. Nagel, Phys. Rev. Lett. **109**, 095704 (2012).

[15] K. VanderWerf, A. Boromand, M. D. Shattuck, and C. S. O'Hern, Phys. Rev. Lett. **124**, 038004 (2020).

[16] S. Chen, T. Bertrand, W. Jin, M. D. Shattuck, and C. S. O'Hern, Phys. Rev. E **98**, 042906 (2018).

[17] P. Morse, S. Wijtmans, M. van Deen, M. van Hecke, and M. L. Manning, Phys. Rev. Research **2**, 023179 (2020).

[18] P. J. Tuckman, K. VanderWerf, Y. Yuan, S. Zhang, J. Zhang, M. D. Shattuck, and C. S. O'Hern, Soft Matter **16**, 9443 (2020).

[19] D. L. Malandro and D. J. Lacks, Phys. Rev. Lett. **81**, 5576 (1998).

[20] C. E. Maloney and A. Lemaître, Phys. Rev. E **74**, 016118 (2006).

[21] H. Mizuno, K. Saitoh, and L. E. Silbert, Phys. Rev. E **93**, 062905 (2016).

[22] A. Zaccone and E. Scossa-Romano, Phys. Rev. B **83**, 184205 (2011).

[23] S. Dagois-Bohy, B. P. Tighe, J. Simon, S. Henkes, and M. van Hecke, Phys. Rev. Lett. **109**, 095703 (2012).

[24] K. Bagi, Mech. Mater. **22**, 165 (1996).

[25] E. Bitzek, P. Koskinen, F. Gähler, M. Moseler, and P. Gumbsch, Phys. Rev. Lett. **97**, 170201 (2006).

[26] R. Lakes, Phys. Rev. Lett. **86**, 2897 (2001).

[27] C. P. Goodrich, S. Dagois-Bohy, B. P. Tighe, M. van Hecke, A. J. Liu, and S. R. Nagel, Phys. Rev. E **90**, 022138 (2014).

[28] W. G. Ellenbroek, E. Somfai, M. van Hecke, and W. van Saarloos, Phys. Rev. Lett. **97**, 258001 (2006).

[29] M. Wyart, Ann. Phys. (Paris, Fr.) **30**, 1 (2005).

[30] E. Somfai, M. van Hecke, W. G. Ellenbroek, K. Shundyak, and W. van Saarloos, Phys. Rev. E **75**, 020301 (2007).

[31] M. Mailman, C. F. Schreck, C. S. O'Hern, and B. Chakraborty, Phys. Rev. Lett. **102**, 255501 (2009).

[32] C. F. Schreck, N. Xu, and C. S. O'Hern, Soft Matter **6**, 2960 (2010).

[33] C. Brito, H. Ikeda, P. Urbani, M. Wyart, and F. Zamponi, Proc. Natl. Acad. Sci. USA **115**, 11736 (2018).